Shear capacity of cold-formed steel channels with edge-stiffened web holes, unstiffened web holes, and plain webs

Chen, Boshan; Roy, Krishanu; Fang, Zhiyuan; Uzzaman, Asraf; Pham, Cao Hung; Raftery, Gary M.; Lim, James B. P.

Published in:
Journal of Structural Engineering (ASCE)

DOI:
10.1061/(asce)st.1943-541x.0003250

Published: 28/02/2022

Shear capacity of cold-formed steel channels with edge-stiffened web holes, un-stiffened web holes and plain webs

Boshan Chen[1], Krishanu Roy[2*], Zhiyuan Fang[3], Asraf Uzzaman[4], Cao Hung Pham[5], Gary M. Raftery[6], James B.P. Lim[7]

[1] Ph.D. Student, Dept. of Civil and Environmental Engineering, Univ. of Auckland, Auckland, New Zealand.
ORCID: https://orcid.org/ /0000-0001-9176-0731. Email: bche719@aucklanduni.ac.nz

[2] Lecturer, Dept. of Civil and Environmental Engineering, Univ. of Auckland, Auckland, New Zealand
ORCID: https://orcid.org/0000-0002-8086-3070. Email: kroy405@aucklanduni.ac.nz

[3] Ph.D. Student, Dept. of Civil and Environmental Engineering, Univ. of Auckland, Auckland, New Zealand.
ORCID: https://orcid.org/0000-0003-1186-5221. Email: zfan995@aucklanduni.ac.nz

[4] Lecturer, School of Computing, Engineering and Physical Sciences, Univ. of the West of Scotland, United Kingdom
ORCID: https://orcid.org/0000-0001-9687-5810. Email: Asraf.Uzzaman@uws.ac.uk

[5] Senior lecturer, School of Civil Engineering, The Univ. of Sydney, Australia
ORCID: https://orcid.org/0000-0002-5503-5839. Email: caohung.pham@sydney.edu.au

[6] Senior Lecturer, Dept. of Civil and Environmental Engineering, Univ. of Auckland, Auckland, New Zealand
ORCID: https://orcid.org/0000-0003-4783-3897. Email: g.raftery@auckland.ac.nz

[7] Associate Professor, Dept. of Civil and Environmental Engineering, Univ. of Auckland, Auckland, New Zealand.
ORCID: https://orcid.org/0000-0001-9720-8518. Email: james.lim@auckland.ac.nz

*Corresponding Author Contact Details:
Krishanu Roy
E: krishanu.roy@auckland.ac.nz, T: +64 223917991, F: +64 9 373 7462, Department of Civil Engineering, University of Auckland, Auckland, New-Zealand-1025

Abstract

In this paper, a total of 254 results comprising 30 shear tests and 224 finite element (FE) analysis results are reported. Simply supported test specimens of cold-formed steel (CFS) channels with aspect ratios of 1.0 and 1.5 were tested. For comparison, specimens with un-stiffened web holes and plain webs were also tested. A nonlinear elasto-plastic FE model was then developed and validated against the experimental results. Using the validated FE model, a parametric study was conducted to investigate the effect of various influential parameters on the shear capacity of such CFS channels. The test and FE results shows that for a channel with edge-stiffened web holes, the shear capacity increased by 13.6% on average, when compared with that of a channel with un-stiffened web holes. The test and FE results were compared against the design predictions. Upon comparison, it was found that the design rules of CFS channels with un-stiffened web holes in accordance with the AISI (2016) and AS/NZS (2018) can be un-conservative by 7%, while calculating the shear capacity of CFS channels with edge-stiffened web holes. Therefore, a suitable design formula in the form of a shear capacity reduction factor was proposed for CFS channels with edge-stiffened web holes.

Keywords

Cold-formed steel, Channels, Shear capacity, Edge-stiffened web holes, Experiments, Finite element analysis

1 Introduction

In recent times, a new generation of cold-formed steel (CFS) channels with edge-stiffened web holes developed by Howick Ltd. (2013) are being widely used in New Zealand (Fig. 1). Such CFS channel members when used as floor joists and bearers are often subjected to concentrated loads, hence experiencing shear failure. However, no work was reported in the literature investigating the shear capacity of CFS channels with edge-stiffened web holes. Furthermore, current design codes, i.e., the American Iron and Steel Institute (AISI) (2016) and the Australian and New Zealand Standards (AS/NZS) (2018) do not provide any design guidance for CFS channels with edge-stiffened web holes.

This paper presents the results of 30 new laboratory tests and 224 finite element analyses (FEA) on CFS channels with edge-stiffened web holes, un-stiffened web holes, and plain webs when subjected to shear. Fig. 2. shows the details of the CFS channels studied in this paper.

Limited work have been reported in the literature studying CFS channels with edge-stiffened web holes under different loading cases (Chen et al. 2020a,b, 2021a; Chi et al. 2021). For compression tests, Chen et al. (2019) experimentally and numerically studied the axial capacity of CFS channels with edge-stiffened web holes and the results suggested that the axial capacity of CFS channels with edge-stiffened web holes performs better than that of a plain channel. Fang et al. (2021a,b) proposed a framework of deep belief network (DBN) for studying the axial capacity of CFS channels with edge-stiffened web holes subject to axial compression. For bending tests, Yu et al. (2012) and Chen et al. (2020c) studied the influence of edge-stiffened web holes on the moment capacity, and the results suggested that edge-stiffened web holes can improve the moment capacity of such channels. In terms of web crippling tests, a recent study by Uzzaman et al. (2017, 2020a,b) and Chen et al. (2021b) suggested that edge-stiffened web holes can also improve web crippling strength of such channels.

In terms of CFS plain channels, significant work has been reported in the literature. The shear behaviour of CFS plain channels was first studied by LaBoube and Yu (1978), and they first proposed suitable design formulas for calculating the shear capacity of CFS plain channels. A study by Keerthan and Mahendran (2015) found that design shear capacity for CFS plain channels determined from AISI (2016) and AS/NZS (2018) are conservative as they did not include the post-buckling strength. Hence, Keerthan and Mahendran (2015) proposed improved shear capacity formulas on the basis of their test and FEA results. Pham and Hancock (2010a, b) experimentally and numerically studied the shear behaviour of high strength CFS channels with and without flange straps. They found that the shear capacities of CFS channels with angle straps are higher than those without flange straps. Also, Pham and Hancock (2009) found that flanges can have a significant effect on the shear buckling capacity of CFS channels.

Regarding CFS channels with un-stiffened web holes, extensive work has been reported on reduced shear capacity of CFS channels with un-stiffened web holes by many researchers. Shan et al. (1997) found that the key parameter for the shear capacity of CFS channels with un-stiffened web holes is the ratio of the depth of web hole (d_{wh}) to clear height of web (d_1) and thus developed shear capacity reduction factors in terms of d_{wh}/d_1. Eiler (1997) extended the research work of Shan et al. (1997) to include the effects of web elements with holes when subjected to varying shear force, which have been adopted in AISI (2016) and AS/NZS (2018). Keerthan and Mahendran (2013b, 2014) experimentally and numerically studied the shear capacity of CFS channels with un-stiffened web holes. They also used the reduction factor and proposed improved design formulas for such sections. To extend the direct strength method (DSM) to CFS channels with un-stiffened web holes in shear, an experimental study was conducted by Pham et al. (2017a, b, 2020a, b, c, d) to study the shear capacity of CFS channels with un-stiffened web holes having an aspect ratio up to 3.0, and they proposed a DSM design approach for CFS members with holes in shear. However, no previous research has studied the shear capacity of CFS channels with edge-stiffened web holes. The issue is addressed in this paper.

As mentioned previously, this paper reports in relation to 30 new laboratory tests on the shear capacity of CFS channels with edge-stiffened web holes, un-stiffened web holes and plain webs. A nonlinear FE model was then developed and validated against the results obtained from laboratory tests in terms of ultimate strength and deformed shapes. A parametric study involving 224 models was conducted based on the validated FE models. To verify the accuracy of current design procedures found in the literature for CFS channels with un-stiffened web holes, the results obtained from laboratory tests and FEA were compared against design predictions of AISI (2016), AS/NZS (2018), Keerthan and Mahendran (2014), and Shan et al. (1997). Finally, a suitable design formula in the form of shear capacity reduction factor was proposed for determining the shear capacity of such CFS channels.

2 Experimental study

2.1 Test specimens

A total of 30 CFS channels in shear were studied in this laboratory tests. Six experiments were conducted on specimens without web holes (Fig.3 (a)), 12 experiments were on specimens with un-stiffened web holes (Fig.3 (b)) and the remaining 12 experiments were conducted on specimens with edge-stiffened web holes (Fig.3 (c)).

To simulate shear boundary conditions, relatively short test beams having two aspect ratios (shear span /clear web height (d_1)) of 1.0 and 1.5 were selected. This paper mainly focused on the shear behaviour of such CFS channel sections with a shear span-to-clear web height ratio of 1.0. However, the influence of combined shear and bending behaviour on the strength and failure modes of such sections were also experimentally investigated (aspect ratios of 1.5).

The test specimens comprised two different section sizes, namely section 240 and section 290. To study the influence of hole sizes on the shear capacity of CFS channels, two different hole diameters (d_{wh}) of 90 and 140 mm were selected.

It should be noted that the web holes are strengthened through a continuous lip around the perimeter of the hole (i.e., with edge-stiffened web hole). As can be seen from Fig.2, the length of the edge-stiffener was fixed at 13 mm. Tables 1 and 2 summarise the measured dimensions of test specimens.

2.2 Section labels

The test specimens were labelled in such a way that the nominal dimensions of web depth, aspect ratio, diameter of holes, the type of web holes, and the flange conditions were identified by the label. For example, the label "240-A1.0-D90-EH-FR" can be interpreted as follows:

- "240" means the nominal dimensions of web depth in millimetres i.e., d=240 mm.
- "A1.0" is the aspect ratio of the channel beams i.e., a/d_1=1.0
- "D90" means the nominal diameter of web holes in millimetres i.e., d_{wh} = 90 mm.
- "EH' identifies a web with edge-stiffened hole, "NH' identifies a plain web, and "UH' means a web with un-stiffened hole.
- "FR" represents the flanges restrained by flange straps.

2.3 Material testing

To obtain the material properties of the test specimens, a total of 6 coupons were prepared, which were cut from the flat portion of the channels, and tested using an Instron tensile testing machine in accordance with the test procedure mentioned in the ISO 6892-1 (ISO 2009) (Fig. 4). The stress-strain curves obtained from the tensile coupon tests for sections 240 and 290 are presented in Figs. 5(a) and (b), respectively. Table 3 shows that the average yield stresses ($\sigma_{0.2}$) for section 240 and 290 are 301.6 MPa and 308.5 MPa, respectively.

2.4 Testing-rig and loading procedure

The concentrated loads were applied using an MTS machine with a capacity of 300 kN at a constant rate of 0.7 mm/min. Two single channels were connected back-to-back by using three numbers of 30mm thick T-shaped stiffeners. The use of twelve 100-mm-wide stiffening plates during the tests was to provide the required simply supported boundary conditions at the supports and at the loading point, while also eliminating the possibility of web crippling failure. A 30-mm gap was incorporated between the two specimens to allow the test beams to buckle independently. To study the influence of flange straps on the shear behaviour and strength, 20 tests were conducted on restrained supports, which were ensured by using eight angle straps at the loading and support points. Additionally, 10 tests were conducted without using any angle strap. Three linear variable differential transformers (LVDTs) were selected to record the vertical displacement of the test specimens. One LVDT was placed under the loading point while the remaining two LVDTs were placed at the support point. The photograph and schematic drawing of the experimental setup are presented in Figs. 6. and 7., respectively.

2.5 Experimental results

Fig. 8. plotted the shear capacity versus displacement curves of all test specimens. The shear capacity was determined as the applied load (P) divided by four, as two back-to-back CFS channels were used. Fig. 9. shows the deformed shapes of the CFS channels with flange straps. From the failure modes, it can be clearly seen that shear failure occurred for all test specimens. The ultimate shear capacity (V_v) obtained from the laboratory tests are summarized in Tables 1 and 2 for fastened flange and unfastened flange cases, respectively. As shown in Tables 1 and 2, for a channel with edge-stiffened

web holes, the shear capacity increased by 13.6% on average, when compared with that of a channel with un-stiffened web holes.

Table 4 summarizes the shear capacity of CFS channels with and without flange straps (i.e., with and without flange restraints). From the results reported in Table 4, it can be confirmed that there is a reduction in shear capacity of CFS channels by 11.04% on average, when the straps were not attached to their flanges. Fig. 10 shows the failure modes of CFS plain channels, when the flanges were not restrained (without flange straps). It can be seen that the flange distortions occurred due to the distortional buckling or unbalanced shear flow in these sections.

The combined shear and bending behaviour can significantly affect the shear capacity for those longer specimens having higher aspect ratios. Table 5 shows the comparison of the shear capacity of specimens having aspect ratios of 1.0 and 1.5. This comparison indicates that shear capacities of those specimens having an aspect ratio of 1.5 were reduced by 24.9% on average due to this combined shear and bending action.

3 Numerical study

3.1 General

ABAQUS (2018) software was used to develop a nonlinear FE model to simulate the CFS channels with and without holes in shear. The measured cross-section dimensions as well as material properties obtained from the tensile coupon tests were incorporated in the FE model. Specific modeling techniques are discussed next.

3.2 Modeling of geometry and material properties

The ABAQUS classical metal plasticity model was selected to define the isotropic yielding and plastic hardening of the steel. The material properties obtained from the tensile coupon tests were incorporated in the FE models. A similar modeling technique was used by Roy et al. (2020) and Li et al. (2019). As per the ABAQUS manual (2018), the engineering material curve was converted into a true material curve by using the following formulas given below:

$$\sigma_{true} = \sigma(1+\varepsilon) \quad (1)$$

$$\varepsilon_{true(pl)} = \ln(1+\varepsilon) - \frac{\sigma_{true}}{E} \quad (2)$$

3.3 FE meshing

S4R shell elements were selected to model the CFS channels. The mesh sensitivity analysis indicated that a mesh size between 5 mm to 10 mm was selected for modeling the CFS channels with and without web holes. For the T-shaped stiffeners, a mesh size of 10 mm × 10 mm was selected. Mesh refinement was selected around the web holes and rounded corners to enable an accurate FE analysis (Fig. 11).

3.4 Boundary conditions and loading procedure

The simply supported boundary conditions were modelled by releasing both the in-plane rotation and axial displacement. The reference points were placed at the top of T-shaped stiffeners. The vertical translation was not restrained at the loading point. The vertical loading was applied by specifying the displacement at the reference loading points. In the FE model, surface-to-surface interaction was used between the webs of each CFS channel. It should be noted that the modeling of bolting connections was simplified to eliminate any possible slippage of the bolts. The experimental results confirmed that the failure of angle straps did not occur when they were used in the tests. Therefore, the angle straps were simulated using suitable boundary conditions. The applied boundary conditions in the FE model are presented in Fig. 12 for the specimen 290-A1.5-D140-EH-FR.

3.5. Modeling of initial geometric imperfections and residual stresses

It should be noted that a value of 0.006d_1 was taken as the magnitude of imperfections in the numerical modeling of CFS channels (Keerthan and Mahendran 2014). The imperfect initial geometries were simulated using the *IMPERFECTION option in the ABAQUS (2018) library. From analysing a limited number of FE models, a decrease of only 1.2% in shear capacity was found when the effects of residual stresses were considered in the FE models, indicating that residual stresses have negligible effect on the shear capacity of CFS channels (Fig. 13). Therefore, the influence of residual stresses on the shear capacity of CFS channels was not considered in the FE models.

3.6 Validation of the finite element model

Table 6 reports the comparison of the laboratory test results (V_{EXP}) with the numerical results (V_{FEA}). The mean value of the V_{EXP} / V_{FEA} ratio is 1.01 with the corresponding coefficient of variation (COV) of 0.07. Fig. 14 presents the deformed shapes at failure from both the laboratory tests and FEA. It can be clearly seen that the deformed shapes determined from the FEA are similar to those determined from the laboratory tests. Fig. 15 plotted shear capacity versus displacement behaviour obtained from both the FEA and laboratory tests for specimens 240-A1.5-D90-UH-FR and 240-A1.5-D90-UH-FU, which shows good agreement between FEA and laboratory test results.

4 Parametric study

A parametric study comprising 224 FE models was undertaken to develop an extensive shear capacity database for CFS channels with edge-stiffened web holes, un-stiffened web holes and plain webs. It should be noted that only aspect ratios of 1.0 were considered in the parametric study section, as the parametric study section only considered the shear behaviour of such sections.

To investigate the influence of web height to web thickness ratio (d_1/t_w) on the shear capacity of such sections, the same FE model was selected with varying web thickness (t_w). The d_1/t_w ratio was thus varied from 96 to 290 by varying the web thickness from 1.0 mm to 2.5 mm, as listed in Table 7. For specimens with holes, the ratio of d_{wh}/d_1 was varied between 0.1 and 0.7 to investigate the influences of hole diameter on the shear capacity of such sections. The ratio of stiffener length to web height (q/d_1) was changed from 0.04 to 0.12. The FE models in the parametric study were coded in such a way that all the geometric parameters could be automatically varied.

Fig. 16(a) and Table 7 show the influence of q/d_1 ratio on the shear capacity of CFS channels with edge-stiffened web holes. The comparison showed that an increase in shear capacity of 11.6% was noticed when q/d_1 ratio was increased from 0.04 to 0.12. It was found that the influence of stiffener length on the shear capacity of such CFS channels cannot be ignored. Fig. 16(b) and Table 7 show the influence of the ratio d_{wh}/d_1 on the shear capacity of CFS channels with edge-stiffened web holes. The comparison results indicated that the ultimate shear capacities were decreased by 53% on average when d_{wh}/d_1 ratio was changed from 0.1 to 0.7, indicating that the influence of d_{wh}/d_1 ratio on the shear capacity of CFS channels was significant.

5 Current shear design rules

5.1 General

Current design rules for calculating the shear capacity of CFS channels with holes are designed on the basis of a reduction factor (q_s), which can be defined as the ratio of nominal shear capacity of CFS channels with holes (V_{nl}) to the nominal shear capacity of CFS channels without holes (V_v). In this section, the currently available design rules for calculating the nominal shear capacity of CFS without holes (V_v) as well as reduction factor (q_s) are discussed next.

5.2 Design rules for CFS channels without web holes in shear

5.2.1 DSM design rules in shear without tension field action

According to Section G2.2 of AISI (2016) and Clause 7.2.3 of AS/NZS (2018), the nominal shear capacity (V_{DSM-1}) of unperforated CFS channel beams without web stiffeners can be calculated using the following Equations (3) to (8).

$$V_v = V_y \quad \text{For } \lambda_v \le 0.815 \tag{3}$$

$$V_v = 0.815\sqrt{V_{cr}V_y} \quad \text{For } 0.815 < \lambda_v \le 1.227 \tag{4}$$

$$V_v = V_{cr} \quad \text{For } \lambda_v > 1.227 \tag{5}$$

$$V_y = 0.6 A_w F_y \tag{6}$$

$$V_{cr} = \frac{0.904 E k_v t_w^3}{d_1} \tag{7}$$

$$\lambda_v = \sqrt{\frac{V_y}{V_{cr}}} \tag{8}$$

5.2.2 DSM design rules in shear with tension field action

Pham and Hancock (2010a, b) conducted both experimental and numerical investigations to propose design formulas for the shear capacity of unperforated CFS channel beams with tension field action (Equations 9 and 10), which have been adopted in Section G2.2 of AISI (2016) and in Clause 7.2.3 of AS/NZS (2018) standards. These formulas (V_{DSM-2}) can closely predict the shear capacity of CFS lipped channels without holes, which accounts for their post-buckling strength and includes the influence of additional fixity on the web-flange junction point.

$$\boldsymbol{V}_v = \boldsymbol{V}_y \quad \text{For, } \lambda_v \le 0.776 \tag{9}$$

$$V_v = \left[1 - 0.15 \left(\frac{V_{cr}}{V_y}\right)^{0.4}\right] \left(\frac{V_{cr}}{V_y}\right)^{0.4} V_y \quad \text{For, } \lambda_v > 0.776 \tag{10}$$

5.2.3 Design rules proposed by Keerthan and Mahendran (2015)

Keerthan and Mahendran (2015) modified the current shear design rules of AS/NZS 4600 (2018) and proposed new formulas as demonstrated in Equations 11, 12 and 13, which include the available post-buckling strength of CFS channels and the additional fixity on the web-flange junction point. The shear buckling coefficient (k_{LCB}) was included to allow for the additional fixity at the web-flange junction of CFS channels, while a post-buckling coefficient of 0.2 was selected in Equations 12 and 13, as shown below:

$$V_v = V_y \quad \text{For, } \frac{d_1}{t_w} \le \sqrt{\frac{E k_{LCB}}{f_y}} \tag{11}$$

$$V_v = V_i + 0.2(V_y - V_i) \quad \text{For, } \sqrt{\frac{E k_v}{f_y}} < \frac{d_1}{t_w} \le 1.508 \sqrt{\frac{E k_{LCB}}{f_y}} \tag{12}$$

$$V_v = V_{cr} + 0.2(V_y - V_{cr}) \quad \text{For, } \frac{d_1}{t_w} \geq 1.508\sqrt{\frac{Ek_{LCB}}{f_y}} \tag{13}$$

5.3 Design rules for CFS channels with un-stiffened web holes in shear

5.3.1 Design rules proposed by Shan et al. (1997)

Shan et al. (1997) concluded that the main parameter influencing the shear capacity is the ratio of depth of the hole to the flat depth of the web (d_{wh}/d_1), and they developed a linear reduction factor for CFS channels with un-stiffened web holes, which incorporated the parameter d_{wh}/d_1. The reduction factor proposed by Shan et al. (1997) can be determined by using Equations 14 and 15:

$$q_s = 1.71 - 3.66\left(\frac{d_{wh}}{d_1}\right) \quad \text{For } \frac{d_{wh}}{d_1} < 0.38 \tag{14}$$

$$q_s = 0.46 - 0.38\frac{d_{wh}}{d_1} \quad \text{For } 0.38 < \frac{d_{wh}}{d_1} \leq 1 \tag{15}$$

5.3.2 Design rules in accordance with the design rules of AISI (2016) and AS/NZS (2018)

The formulas for determining the shear capacity reduction factor are presented in AISI (2016) and AS/NZS (2018) for CFS channels with un-stiffened web holes on the basis of the research findings of Eiler et al. (1997), who suggested that the reduction of shear capacity due to the presence of web holes can be estimated by applying a reduction factor to the nominal shear capacity of the plain web. The shear capacity reduction factor formulas developed by Eiler et al. (1997), which are available in AISI (2016) and AS/NZS (2018) can be determined by using Equations 16 to 20:

$$q_s = 1 \quad \text{For } \frac{c}{t} > 54 \tag{16}$$

$$q_s = \frac{c}{54t} \quad \text{For } 5 < \frac{c}{t} < 54 \tag{17}$$

$$c = \frac{d_1}{2} - \frac{d_{wh}}{2.83} \tag{18}$$

$$\frac{d_{wh}}{d_1} \leq 0.7 \tag{19}$$

$$\frac{d_1}{t} \leq 200 \tag{20}$$

5.3.3 Design rules proposed by Keerthan and Mahendran (2013b, 2014)

Keerthan and Mahendran (2013b, 2014) experimentally and numerically studied the shear capacity of CFS channels with un-stiffened web holes. From the outcome of their research, they proposed shear capacity reduction factors due to the presence of web holes. Based on their recommendation, shear capacity of CFS channels with un-stiffened web holes (V_{nl}) can be calculated using a reduction factor q_s, which is normally applied to the shear capacity of plain channels (V_v). Equations 21 to 23 present the proposed design formulas for the shear capacity reduction factor of perforated CFS channel sections.

$$q_s = 1 - 0.6(\frac{d_{wh}}{d_1}) \quad \text{For } 0 < \frac{d_{wh}}{d_1} < 0.3 \tag{21}$$

$$q_s = 1.215 - 1.316(\frac{d_{wh}}{d_1}) \quad \text{For } 0.3 < \frac{d_{wh}}{d_1} < 0.7 \tag{22}$$

$$q_s = 0.732 - 0.625(\frac{d_{wh}}{d_1}) \quad \text{For } 0.7 < \frac{d_{wh}}{d_1} < 0.85 \tag{23}$$

6. Comparison of tests and FE results with design strengths

The results obtained from laboratory tests and FEA were in comparison with the design shear capacities determined from the design rules of AISI (2016), AS/NZS (2018), Pham and Hancock (2010a, b) and Keerthan and Mahendran (2015) for CFS plain channels. The comparison results are reported in Table 8 and plotted in Fig.17. The DSM design rules in shear without tension field action as per the AISI (2016) and AS/NZS (2018), are overly conservative, as they do not include the influence of post-buckling strength. However, the DSM design rules in shear with tension field action proposed by Pham and Hancock (2010a, b) was close to the results obtained from laboratory tests. The results obtained from the formulas proposed by Keerthan and Mahendran (2015) are conservative by 18% on average, when compared with the results obtained from the laboratory tests.

The shear capacities of CFS channels with un-stiffened web holes obtained from the laboratory tests and FEA are in comparison with the predictions from the currently available design rules as shown in Table 9. The comparison results show that the shear capacities determined from Shan et al.'s (1997) design formulas are over conservative by 62% on average. The design formulas in accordance with the AISI (2016) and AS/NZS (2018) are conservative mostly for CFS channels with small web holes, while they are un-conservative for channels with larger web holes, which was also reported by Keerthan and Mahendran (2013b, 2014). This comparison shows that the shear capacities determined from Keerthan and Mahendran's (2013b, 2014) design formulas are conservative by 7% on average. Fig. 18 shows the non-dimensional curve of q_s versus $d_{wh}/d_{1.}$

For CFS channels with edge-stiffened web holes, the shear capacity reduction factors obtained from laboratory tests and FEA were in comparison with those obtained from the design formulas of CFS channels with un-stiffened web holes. The comparison results are presented in Table 10, indicating that the design formulas in accordance with the AISI (2016) and AS/NZS (2018) are un-conservative by 7% on average. This is due to the fact that the current design rules of CFS channels with web holes do not consider the effects of edge-stiffener. Therefore, new design rules for CFS channels with edge-stiffened web holes should be developed.

7. Proposed design formulas

New design rules in the form of a reduction factor were proposed in this paper to determine the shear capacity of CFS channels with edge-stiffened web holes, based on the experimental and numerical results presented herein. It should be noted that a previous study reported by the same authors (Chen et al. 2020c) indicated that the influences of r_q/t_w ratio on the capacity of such CFS channels are limited. Therefore, the ratio r_q/t_w was not considered in the proposed design formulas. Only the primary influencing parameters such as, q/d_1 and d_{wh}/d_1 ratios were considered. The design formulas for calculating the shear capacity reduction factors ($q_{s(pr)}$) of CFS channels with edge-stiffened web holes are given next.

$$q_{s(pr)} = 1.04 + 0.67\frac{q}{d_1} - 0.59\frac{d_{wh}}{d_1} \qquad \text{For, } 0.1 \leq d_{wh}/d_1 \leq 0.3 \qquad (24)$$

$$q_{s(pr)} = 1.42 + 1.08\frac{q}{d_1} - 1.59\frac{d_{wh}}{d_1} \quad \text{For, } 0.3 < d_{wh}/d_1 \leq 0.5 \quad (25)$$

$$q_{s(pr)} = 1.72 + 1.18\frac{q}{d_1} - 1.91\frac{d_{wh}}{d_1} \quad \text{For, } 0.5 < d_{wh}/d_1 \leq 0.7 \quad (26)$$

The validity for the proposed design formulas shall apply within the following limits: (a)$0.1 \leq d_{wh}/d_1 \leq 0.7$; (b) $0.04 \leq q/d_1 \leq 0.12$; (c) $96 \leq d_1/t_w \leq 290$

In order to assess the accuracy of the proposed design formulas for a shear capacity reduction factor of CFS channels with edge-stiffened web holes (Equations (24)-(26)), Fig. 19 and Table 10 compare their predictions with the corresponding results obtained from laboratory tests and FEA. From the comparison results, it was found that the shear capacity reduction factor determined from Equations (24) to (26) agree well with the results obtained from laboratory tests and FEA.

8. Reliability analysis

A reliability analysis was carried out to assess the reliability of the proposed design formulas for determining the shear capacity reduction factors of CFS channels with edge-stiffened web holes. A target reliability index of 2.5 for CFS structural members is recommended as a lower limit in the AISI Specification (2016). Design formulas are considered reliable if the value of the reliability index (β) is greater than or equal to 2.5 (AISI, 2016). A load combination of 1.2DL+1.6LL as specified in the AISI Specification (2016) was used in the reliability analysis. In the calculation, DL means the dead load, while LL means the live load. The statistical parameters were determined from the AISI Specification (2016) for CFS members, where M_m = 1.10, F_m = 1.00, V_M = 0.10, and V_F= 0.05. These values are the mean values and coefficients of variations for material and fabrication properties.

Table 11 confirms that the values of β are 2.84, 2.80 and 2.80, for Equations 24, 25 and 26, respectively, indicating that the proposed design formulas are reliable for determining the shear capacity reduction factor of CFS channels with edge-stiffened web holes.

9. Concluding remarks

This paper presents the details of an experimental and numerical investigation into the shear capacity of CFS channels with edge-stiffened web holes, un-stiffened web holes and plain webs. A total of 254 results comprising 30 laboratory tests and 224 FE results are reported.

The results obtained from laboratory tests indicate that for a channel with edge-stiffened web holes, the shear capacity increased by 13.6% on average, when compared with that of a channel with un-stiffened web holes. Also, CFS channels without flange restraints had an 11.04% lower shear capacity than its restrained equivalent. The shear capacities of those specimens with an aspect ratio of 1.5 were reduced by 24.9% on average due to this combined action.

A numerical model is then developed and validated against the corresponding results obtained from laboratory tests, which showed good agreement both in terms of ultimate strength and failure modes.

A parametric study comprising 224 FE models was conducted based on the validated FE models

The current design formulas in AISI (2016) and AS/NZS (2018) for web holes are demonstrated to be un-conservative by 7% on average when determining the shear capacity reduction factor of such CFS channels with edge-stiffened web holes.

Modified design formulas are therefore proposed using bivariate linear regression analysis. A reliability analysis was carried out to assess the proposed design formulas, indicating that the proposed design formulas can closely determine the shear capacity reduction factor of CFS channels with edge-stiffened web holes.

Data Availability Statement

All of the data and models generated or used during the study appear in the submitted article.

Acknowledgements

Test specimens were provided by Howick NZ. Ltd. and this is greatly acknowledged by the authors. The shear tests were carried out at University of Auckland.

References

ABAQUS version 6.14-2 [Computer software]. Dassault Systemes, Waltham, MA, 2018.

American Iron and Steel Institute (AISI) 2016. "North American specification for the design of cold-formed steel structural members, 2016 Edition." AISI S100-16w*,* Washington, DC. USA.

Australia/New Zealand Standard (AS/NZS). 2018. "Cold-Formed Steel Structures, AS/NZS 4600:2018." Joint Technical Committee, Sydney.

Chen, B., K. Roy, A. Uzzaman, G.M. Raftery, D. Nash, G. C. Clifton, P. Pouladi, and J.B.P. Lim. 2019. "Effects of edge-stiffened web openings on the behaviour of cold-formed steel channel sections under compression." *Thin-Walled Struct*. 144:106307. https://doi.org/10.1016/j.tws.2019.106307.

Chen, B., K. Roy, A. Uzzaman, G.M. Raftery, and J.B.P. Lim. 2020a. "Parametric study and simplified design equations for cold-formed steel channels with edge-stiffened holes under axial compression." *J. Constr. Steel Res*., 172:106161. https://doi.org/10.1016/j.jcsr.2020.106161.

Chen, B., K. Roy, A. Uzzaman, G.M. Raftery, and J.B.P. Lim. 2020b. "Axial strength of back-to-back cold-formed steel channels with edge-stiffened holes, un-stiffened holes and plain webs" *J. Constr. Steel Res*., 174:106313. https://doi.org/10.1016/j.jcsr.2020.106313.

Chen, B., K. Roy, A. Uzzaman, and J.B.P. Lim. 2020c. "Moment capacity of cold-formed channel beams with edge-stiffened web holes, un-stiffened web holes and plain webs." *Thin-Walled Struct*. 157:107070. https://doi.org/10.1016/j.tws.2020.107070.

Chen, B., K. Roy, Z. Fang, A. Uzzaman, G.M. Raftery, and J.B.P. Lim. 2021a. "Moment capacity of back-to-back cold-formed steel channels with edge -stiffened hole, un-stiffened hole, and plain web" *Eng. Struct.*, 235:112042. https://doi.org/10.1016/j.engstruct.2021.112042.

Chen, B., K. Roy, Z. Fang, A. Uzzaman, Y. Chi, and J.B.P. Lim. 2021b. "Web crippling capacity of fastened cold-formed steel channels with edge-stiffened web holes, un-stiffened web holes and plain webs under two-flange loading." *Thin-Walled Struct*. 163:107666. https://doi.org/10.1016/j.tws.2021.107666.

Chi, Y., K. Roy, B. Chen, Z. Fang, A. Uzzaman, and J.B.P. Lim, 2021."The effect of opening spacing on the axial capacity of built-up cold-formed steel channel sections with edge-stiffened web holes" *Steel Compos. Struct.,* 40(2):287-305. http://dx.doi.org/10.12989/scs.2021.40.2.287.

Eiler, M.R., R. Laboube, and W.W. Yu, 1997. "Behaviour of web elements with openings subjected to linearly varying shear." Univ. of Missouri-Rolla, Rolla, USA

Fang, Z., K. Roy, B. Chen, C.W. Sham, I. Hajirasouliha, and J.B.P.Lim. 2021a. "Deep learning-based procedure for structural design of cold-formed steel channel sections with edge-stiffened and un-stiffened holes under axial compression" *Thin-Walled Struct*. 166:108076. https://doi.org/10.1016/j.tws.2021.108076.

Fang, Z., K. Roy, J. Mares, C.W. Sham, B. Chen, and J.B.P.Lim. 2021b. "Deep learning-based axial capacity prediction for cold-formed steel channel sections using Deep Belief Network" *Struct*. 33: 2792-2802. https://doi.org/10.1016/j.istruc.2021.05.096.

Howick (2013). Floor joist system. Auckland, New Zealand.

ISO E. 6892-1. 2009. "Metallic Materials: Tensile Testing: Part 1: Method of Test at Room Temperature" ISO E. 6892-1, International Standard, Geneva.

Keerthan, P., and M. Mahendran. 2013a. "Shear buckling characteristics of cold-formed steel channel beams." *Int J Steel Struct.*,13: 385-399. https://doi-org.ezproxy.auckland.ac.nz/10.1007/s13296-013-3001-6.

Keerthan, P., and M. Mahendran. 2013b. "Experimental studies of the shear behaviour and strength of lipped channel beams with web openings." *Thin-Walled Struct*., 73: 131-144. https://doi.org/10.1016/j.tws.2013.06.018.

Keerthan, P., and M. Mahendran. 2013c. “New design rules for the shear strength of litesteel beams with web openings.”. *J. Struct. Eng.*, 139(5): 640-656. https://doi.org/10.1061/(ASCE)ST.1943-541X.0000563.

Keerthan, P., and M. Mahendran. 2014. “Improved shear design rules for lipped channel beams with web openings.” *J. Constr. Steel Res*., 97: 127-142. https://doi.org/10.1016/j.jcsr.2014.01.011.

Keerthan, P., and M. Mahendran. 2015. “Experimental investigation and design of lipped channel beams in shear.” *Thin-Walled Struct*., 86: 174-184. https://doi.org/10.1016/j.tws.2014.08.024

LaBoube, R.A, and Yu W.W. 1978. “Strength of cold-formed steel beam webs in bending, shear, and a combination of bending and shear.” Rolla, USA: American Iron and Steel Institute, University of Missouri-Rolla.

Li, H.T., and B. Young. 2019. “Cold-formed high-strength steel tubular structural members under combined bending and bearing.” *J. Struct. Eng*., 145(8): 04019081. https://doi.org/ 10.1061/(ASCE)ST.1943-541X.0002371.

Pham, C.H., and G.J. Hancock. 2009. “Shear buckling of thin-walled channel sections.” *J. Constr. Steel Res*., 65: 578-585. https://doi.org/10.1016/j.jcsr.2016.10.013.

Pham, C.H., and G.J. Hancock. 2010a. “Experimental investigation of high strength C-sections in combined bending and shear.” *J. Struct. Eng.*, 136: 866-878. https://doi.org/10.1061/(ASCE)ST.1943-541X.0000172.

Pham, C.H., and G.J. Hancock. 2010b. “Numerical simulation of high strength cold-formed purlins in combined bending and shear.” *J. Constr. Steel Res*., 66: 1205-1217. https://doi.org/10.1016/j.jcsr.2010.04.014

Pham, C.H., and G.J. Hancock. 2012. “Direct strength design of cold-formed C-sections for shear and combined actions.” *J Struct Eng*, 138: 759-768. https://doi.org/10.1061/(ASCE)ST.1943-541X.0000510.

Pham, S. H., C. H. Pham, and G. J. Hancock. 2017a. “Direct strength method of design for channel sections in shear with square and circular web holes,” *J. Struct. Eng.*, 143(6): 04017017. https://doi.org/10.1061/(ASCE)ST.1943-541X.0001765.

Pham, C.H. 2017b. “Shear buckling of plates and thin-walled channel sections with holes.” *J. Constr. Steel Res.,* 128: 800-811. https://doi.org/10.1016/j.jcsr.2016.10.013.

Pham, S.H, C.H. Pham, C.A. Rogers, and G.J. Hancock. 2020a. “Shear strength experiments and design of cold-formed steel channels with web holes.” *J. Struct. Eng.*, 146(1): 04019173. https://doi.org/10.1061/(ASCE)ST.1943-541X.0002464.

Pham, C.H., and G. J. Hancock. 2020b. “Shear tests and design of cold-formed steel channels with central square holes.” *Thin–Walled Struct*. 149: 106650. https://doi.org/10.1016/j.tws.2020.106650.

Pham, D.K, C.H. Pham, S.H. Pham and G. J. Hancock. 2020c. “Experimental investigation of high strength cold-formed channel sections in shear with rectangular and slotted web openings.” *J. Constr. Steel Res.,* 165:105889. https://doi.org/10.1016/j.jcsr.2019.105889.

Pham, D.K, C.H. Pham and G. J. Hancock. 2020d. “Parametric study for shear design of cold-formed channels with elongated web openings.” *J. Constr. Steel Res.,* 172: 106222. https://doi.org/10.1016/j.jcsr.2020.106222.

Roy ,K., H.H. Lau, T.C.H. Ting, B. Chen, and J.B.P. Lim. 2020. “Flexural capacity of gapped built-up cold-formed steel channel sections including web stiffeners” *J. Constr. Steel Res.,* 172: 106154. https://doi.org/10.1016/j.jcsr.2020.106154.

Shan, M.Y., R.A. LaBoube, J.E. Langan, and W.W. Yu. 1997. “Cold-formed steel webs with openings: summary report.” *Thin-Walled Struct*., 27: 79-84. https://doi.org/10.1016/0263-8231(96)00021-3

Uzzaman, A, J.B.P. Lim, D. Nash, and B. Young. 2017. “Effects of edge-stiffened circular web openings on the web crippling strength of cold-formed steel channel beams under one-flange loading conditions.” *Eng. Struct.,* 139: 96-107. https://doi.org/10.1016/j.engstruct.2017.02.042.

Uzzaman, A, J.B.P. Lim, D. Nash, and K. Roy. 2020a. “Cold-formed steel channel beams under end-two-flange loading condition: Design for edge-stiffened holes, unstiffened holes and plain webs.” *Thin-Walled Struct.,* 147: 106532. https://doi.org/10.1016/j.tws.2019.106532.

Uzzaman, A, J.B.P. Lim, D. Nash, and K. Roy. 2020b. “Web crippling behaviour of cold-formed steel channel sections with edge-stiffened and unstiffened circular holes under interior-two-flange loading condition.” *Thin-Walled Struct.,* 154: 106813. https://doi.org/10.1016/j.tws.2020.106813.

Yu, C. 2012. “Cold-formed steel flexural member with edge stiffened web openings: behavior, optimization, and design.” *J. Constr. Steel Res*., 71: 210-218. https://doi.org/10.1016/j.jcsr.2011.09.008.

Nomenclature

a	Shear span;
b_f	Width of flange;
b_l	Width of lip;
COV	Coefficient of variation;
CFS	Cold-formed steel;
d_1	Clear height of web;
d_{wh}	Diameter of web hole;
E	Young's modulus of elasticity;
FEA	Finite element analysis;
f_{y}	Yield strength;
L	Total length of test specimen;
LVDTs	Linear variable displacement transducers;
q	Length of stiffener;
q_{s}	Reduction factor;
$q_{\mathrm{s(AISI\&AS/NZS)}}$	Reduction factor predicted from AISI (2016) and AS/NZS (2018)
$q_{\mathrm{s(Shan)}}$	Reduction factor predicted from design rules proposed by Shan et al. (1997)
$q_{\mathrm{s(KM)}}$	Reduction factor predicted from design rules proposed by Keerthan and Mahendran et al. (2013b, 2014);
r_{i}	Inside corner radius of section;
t_{w}	Thickness of web;
$V_{\mathrm{DSM-1}}$	Shear capacity predicted from the DSM design rules in shear without TFA;
$V_{\mathrm{DSM-2}}$	Shear capacity predicted from the DSM design rules in shear with TFA;
V_{EXP}	Shear capacity predicted from laboratory tests;
$V_{\mathrm{EXP-1.0}}$	Experimental shear capacity of specimens with aspect ratios of 1.0;
$V_{\mathrm{EXP-1.5}}$	Experimental shear capacity of specimens with aspect ratios of 1.5;
V_{FEA}	Shear capacity predicted from finite element (FEA);
V_{KM}	Shear capacity predicted from the design equations proposed by Keerthan and Mahendran et al. (2015);
$\sigma_{0.2}$	Static 0.2% proof stress;
σ_{u}	Static ultimate tensile strength;
σ_{true}	True stress ;
$\varepsilon_{\mathrm{true(pl)}}$	True strain ;

Table 1. Measured dimensions and shear capacity for specimens with flanges restrained by straps

a) Section 240

Specimen	Web height	Total length	Web thickness	Stiffener length	Hole diameter	Aspect ratio	Ratio	Ratio	Shear capacity obtained from test	Reduction factor
	d_1	L	t_w	q	d_{wh}	a/d_1	d_1/t_w	d_{wh}/d_1	V_{EXP}	q_s
	(mm)	(mm)	(mm)	(mm)	(mm)				(kN)	
Plain section										
240-A1.0-D0-NH-FR	239.3	672.6	1.81	-	-	1.0	132.2	-	53.7	1.00
240-A1.5-D0-NH-FR	239.3	908.9	1.81	-	-	1.5	132.2	-	37.5	1.00
Edge-stiffened holes										
240-A1.0-D140-EH-FR	236.5	672.6	1.86	13	148.5	1.0	127.2	0.63	35.3	0.66
240-A1.5-D140-EH-FR	238.3	908.9	1.86	13	147.5	1.5	128.1	0.62	31.2	0.83
240-A1.0-D90-EH-FR	239.3	672.6	1.85	13	98.0	1.0	129.4	0.41	49.1	0.91
240-A1.5-D90-EH-FR	238.5	908.9	1.85	13	97.5	1.5	128.9	0.41	37.5	1.00
Un-stiffened holes										
240-A1.0-D140-UH-FR	235.5	672.6	1.86	-	149.5	1.0	126.6	0.63	30.4	0.56
240-A1.5-D140-UH-FR	235.1	908.9	1.85	-	148.2	1.5	127.1	0.63	24.9	0.66
240-A1.0-D90-UH-FR	235.5	672.6	1.88	-	98.0	1.0	125.3	0.42	45.3	0.84
240-A1.5-D90-UH-FR	235.5	908.9	1.88	-	98.5	1.5	125.3	0.42	33.4	0.89

b) Section 290

Specimen	Web height	Total length	Web thickness	Stiffener length	Hole diameter	Aspect ratio	Ratio	Ratio	Shear capacity obtained from test	Reduction factor
	d_1	L	t_w	q	d_{wh}	a/d_1	d_1/t_w	d_{wh}/d_1	V_{EXP}	q_s
	(mm)	(mm)	(mm)	(mm)	(mm)				(kN)	
Plain section										
290-A1.0-D0-NH-FR	289.6	771.2	2.10	-	-	1.0	137.9	-	73.1	1.00
290-A1.5-D0-NH-FR	285.6	1056.	2.11	-	-	1.5	135.4	-	49.1	1.00
Edge-stiffened holes										
290-A1.0-D140-EH-FR	287.6	771.2	2.15	13	148.3	1.0	133.8	0.52	55.9	0.76
290-A1.5-D140-EH-FR	288.5	1056.	2.13	13	147.5	1.5	135.4	0.51	50.0	0.92
290-A1.0-D90-EH-FR	285.6	771.2	2.16	13	98.5	1.0	132.2	0.34	64.8	0.88
290-A1.5-D90-EH-FR	287.0	1056.	2.16	13	99.0	1.5	132.9	0.34	51.3	0.94
Un-stiffened holes										
290-A1.0-D140-UH-FR	285.0	771.2	2.18	-	148.5	1.0	130.7	0.52	51.2	0.70
290-A1.5-D140-UH-FR	286.5	1056.	2.17	-	149.5	1.5	132.0	0.52	42.1	0.86
290-A1.0-D90-UH-FR	285.0	771.2	2.18	-	99.5	1.0	130.7	0.35	63.9	0.87
290-A1.5-D90-UH-FR	285.6	1056.	2.17	-	99.0	1.5	131.6	0.35	48.1	0.98

Table 2. Measured dimensions and shear capacity for specimens with flanges unrestrained by straps

Specimen	Web height	Total length	Web thickness	Stiffener length	Hole diameter	Aspect ratio	Ratio	Ratio	Shear capacity obtained from test	Reduction factor
	d_1	L	t_w	q	d_{wh}	a/d_1	d_1/t_w	d_{wh}/d_1	V_{EXP}	q_s
	(mm)	(mm)	(mm)	(mm)	(mm)				(kN)	
Plain section										
240-A1.0-D0-NH-FU	235.3	672.6	1.85	-	-	1.0	127.1	-	46.9	1.00
240-A1.5-D0-NH-FU	236.3	908.9	1.85	-	-	1.5	127.7	-	35.0	1.00
Edge-stiffened holes										
240-A1.0-D140-EH-FU	237.3	672.6	1.86	13	148.9	1.0	127.6	0.63	31.7	0.67
240-A1.5-D140-EH-FU	238.3	908.9	1.85	13	147.5	1.5	128.8	0.62	28.7	0.82
240-A1.0-D90-EH-FU	235.5	672.6	1.87	13	96.5	1.0	125.9	0.41	41.0	0.87
240-A1.5-D90-EH-FU	237.3	908.9	1.85	13	93.5	1.5	128.3	0.39	35.2	1.01
Un-stiffened holes										
240-A1.0-D140-UH-FU	237.3	672.6	1.86	-	148.5	1.0	127.6	0.63	26.0	0.55
240-A1.5-D140-UH-FU	238.0	908.9	1.86	-	147.0	1.5	128.0	0.62	22.8	0.65
240-A1.0-D90-UH-FU	237.5	672.6	1.87	-	98.0	1.0	127.0	0.41	36.0	0.78
240-A1.5-D90-UH-FU	238.9	908.9	1.85	-	97.5	1.5	129.1	0.41	30.7	0.88

Table 3. Material properties of specimens obtained from tensile coupon tests

Section	Coupon ID	Thickness	Yield stress	Ultimate stress
		t_w/mm	$\sigma_{0.2}$/MPa	σ_u/MPa
Section 240	240-1	1.81	302.3	372.8
	240-2	1.82	300.9	380.1
	240-3	1.81	301.2	383.9
	Mean	1.81	301.6	378.9
Section 290	290-1	2.11	310.2	383.1
	290-2	2.10	308.6	387.4
	290-3	2.13	306.5	390.6
	Mean	2.11	308.5	387.0

Table 4. Comparison of shear capacity of specimens with and without flange restraints

Specimen	Shear capacity predicted from test		Capacity reduction
	With straps	Without straps	
	(kN)	(kN)	(%)
240-A1.0-D0-NH	53.7	46.9	12.6
240-A1.5-D0-NH	37.5	35.0	6.7
240-A1.0-D140-EH	35.3	31.7	10.2
240-A1.5-D140-EH	31.2	28.7	8.0
240-A1.0-D90-EH	49.1	41.0	16.5
240-A1.5-D90-EH	37.5	35.2	6.1
240-A1.0-D140-UH	30.4	26.0	13.3
240-A1.5-D140-UH	24.9	22.8	8.4
240-A1.0-D90-UH	45.3	36.0	20.5
240-A1.5-D90-UH	33.4	30.7	8.1
Mean			11.04

Table 5. Comparison of shear capacity of specimens having aspect ratios of 1.0 and 1.5

Specimen	Shear capacity predicted from test		Capacity reduction
	a/d_1=1.0	a/d_1=1.5	
	$V_{EXP\text{-}1.0}$ (kN)	$V_{EXP\text{-}1.5}$ (kN)	(%)
240-D0-NH-FR	53.7	37.5	43.2
290-D0-NH-FR	73.1	49.1	48.9
240-D0-NH-FU	46.9	35.0	34.0
240-D140-EH-FR	35.3	31.2	13.1
240-D90-EH-FR	49.1	37.5	30.9
290-D140-EH-FR	55.9	50.0	11.8
290-D90-EH-FR	64.8	51.3	26.3
240-D140-EH-FU	31.7	28.7	10.5
240-D90-EH-FU	41.0	35.2	16.5
240-D140-UH-FR	30.4	24.9	18.1
240-D90-UH-FR	45.3	33.4	35.6
290-D140-UH-FR	51.2	42.1	21.6
290-D90-UH-FR	63.9	48.1	32.8
240-D140-UH-FU	26.0	22.8	14.0
240-D90-UH-FU	36.0	30.7	17.3
Mean			24.9

Table 6. Comparison of shear capacity obtained from tests and FEA for all test specimens

Specimen	Aspect	Ratio	Ratio	Shear capacity		Test/FEA
	a/d_1	d_1/t_w	d_{wh}/d_1	Test	FEA	
				(kN)	(kN)	
Plain section						
240-A1.0-D0-NH-FR	1.0	132.2	-	53.7	50.6	1.06
240-A1.5-D0-NH-FR	1.5	132.2	-	37.5	38.3	0.98
240-A1.0-D0-NH-FU	1.0	132.2	-	46.9	49.5	0.95
240-A1.5-D0-NH-FU	1.5	127.7	-	35.0	38.0	0.92
290-A1.0-D0-NH-FR	1.0	137.9	-	73.1	70.7	1.03
290-A1.5-D0-NH-FR	1.5	135.4	-	49.1	53.5	0.92
Edge-stiffened holes						
240-A1.0-D140-EH-FR	1.0	127.2	0.63	35.3	32.1	1.10
240-A1.5-D140-EH-FR	1.5	128.1	0.62	31.2	30.3	1.03
240-A1.0-D90-EH-FR	1.0	129.4	0.41	49.1	46.0	1.07
240-A1.5-D90-EH-FR	1.5	128.9	0.41	37.5	40.1	0.94
240-A1.0-D140-EH-FU	1.0	127.6	0.63	31.7	31.3	1.01
240-A1.5-D140-EH-FU	1.5	128.8	0.62	28.7	29.1	0.99
240-A1.0-D90-EH-FU	1.0	125.9	0.41	41.0	44.4	0.92
240-A1.5-D90-EH-FU	1.5	128.3	0.39	35.2	37.9	0.93
290-A1.0-D140-EH-FR	1.0	133.8	0.52	55.9	51.5	1.09
290-A1.5-D140-EH-FR	1.5	135.4	0.51	50.0	44.9	1.11
290-A1.0-D90-EH-FR	1.0	132.2	0.34	64.8	68.2	0.95
290-A1.5-D90-EH-FR	1.5	132.9	0.34	51.3	55.3	0.93
Un-stiffened holes						
240-A1.0-D140-UH-FR	1.0	126.6	0.63	30.4	28.3	1.07
240-A1.5-D140-UH-FR	1.5	127.1	0.63	24.9	22.7	1.10
240-A1.0-D90-UH-FR	1.0	125.3	0.42	45.3	43.1	1.05
240-A1.5-D90-UH-FR	1.5	125.3	0.42	33.4	34.0	0.98
240-A1.0-D140-UH-FU	1.0	127.6	0.63	26.0	24.0	1.08
240-A1.5-D140-UH-FU	1.5	128.0	0.62	22.8	21.4	1.07
240-A1.0-D90-UH-FU	1.0	127.0	0.41	36.0	38.3	0.94
240-A1.5-D90-UH-FU	1.5	129.1	0.41	30.7	32.0	0.96
290-A1.0-D140-UH-FR	1.0	130.7	0.52	51.2	43.2	1.18
290-A1.5-D140-UH-FR	1.5	132.0	0.52	42.1	38.0	1.11
290-A1.0-D90-UH-FR	1.0	130.7	0.35	63.9	63.9	1.00
290-A1.5-D90-UH-FR	1.5	131.6	0.35	48.1	51.9	0.93
Mean						1.01
COV						0.07

Table 7. Shear capacity predicted from the parametric study for varying thickness, hole diameter ratio and stiffener length ratio (aspect ratio=1.0)

(a) Section 240

Thickness	Hole ratio	Shear capacity obtained from the parametric study, V_{FEA} (kN)						
				With edge-stiffened hole				
t_w (mm)	A (d_{wh}/d_1)	Without hole	With un-stiffened hole	Q0.04	Q0.06	Q0.08	Q0.10	Q0.12
1.0	0.1	22.1	22.0	22.3	22.6	22.8	23.1	23.6
1.0	0.3	22.1	17.8	19.1	19.4	19.9	20.1	20.4
1.0	0.5	22.1	11.7	14.2	14.6	15.3	15.9	16.2
1.0	0.7	22.1	6.6	9.4	9.7	10.2	11.1	11.8
1.5	0.1	40.4	38.1	40.2	40.6	41.0	41.8	42.8
1.5	0.3	40.4	32.4	35.5	35.8	36.1	37.1	37.9
1.5	0.5	40.4	21.0	27.0	28.0	29.0	29.7	30.5
1.5	0.7	40.4	12.1	18.0	18.7	19.7	20.2	20.9
2.0	0.1	56.5	56.4	56.9	57.3	58.0	58.3	58.8
2.0	0.3	56.5	48.3	49.1	49.9	50.6	51.5	52.5
2.0	0.5	56.5	32.2	39.7	40.7	41.9	42.6	43.5
2.0	0.7	56.5	19.6	25.4	26.3	27.4	28.6	29.5
2.5	0.1	86.1	85.6	86.9	87.7	88.6	89.4	90.4
2.5	0.3	86.1	69.2	73.1	74.4	75.9	77.2	78.8
2.5	0.5	86.1	45.5	54.4	56.1	57.7	59.3	60.8
2.5	0.7	86.1	27.0	36.7	38.3	39.6	41.1	42.7

(a) Section 290

Thickness	Hole ratio	Shear capacity obtained from the parametric study, V_{FEA} (kN)						
				With edge-stiffened hole				
t_w (mm)	A (d_{wh}/d_1)	Without hole	With un-stiffened hole	Q0.04	Q0.06	Q0.08	Q0.10	Q0.12
1.0	0.1	25.1	24.7	25.5	25.7	26.1	26.6	26.8
1.0	0.3	25.1	20.7	22.5	22.7	23.2	23.7	24.0
1.0	0.5	25.1	14.6	17.2	17.6	18.0	18.6	19.0
1.0	0.7	25.1	9.1	11.1	11.7	12.4	13.3	13.8
1.5	0.1	46.2	44.7	46.8	47.2	47.7	48.3	48.9
1.5	0.3	46.2	37.4	42.0	42.5	43.2	43.8	44.6
1.5	0.5	46.2	24.9	29.5	30.9	32.3	33.7	35.1
1.5	0.7	46.2	15.1	20.3	21.5	22.8	24.1	25.5
2.0	0.1	66.5	66.0	67.3	68.0	68.8	69.6	70.5
2.0	0.3	66.5	56.7	60.8	61.6	62.6	63.5	64.5
2.0	0.5	66.5	37.4	45.5	47.2	48.7	50.3	52.1
2.0	0.7	66.5	22.7	29.5	31.5	33.3	35.5	37.5
2.5	0.1	90.5	89.7	91.5	92.5	93.3	94.5	95.5
2.5	0.3	90.5	74.0	82.0	83.2	84.2	85.3	86.5
2.5	0.5	90.5	52.1	61.1	63.2	65.1	66.8	68.9
2.5	0.7	90.5	32.3	39.2	41.6	43.7	46.2	48.5

Table 8. Comparison of shear capacity obtained from tests, parametric study and current design formulae for CFS plain channels (aspect ratio=1.0)

Specimen	Thickness	Ratio	Shear capacity (kN)				Comparison		
	t_w (mm)	d_1/t_w	$V_{EXP\&FEA}$	V_{DSM-1}	V_{DSM-2}	V_{KM}	$V_{EXP\&FEA}/V_{DSM-1}$	$V_{EXP\&FEA}/V_{DSM-2}$	$V_{EXP\&FEA}/V_{KM}$
Experiments									
240-D0-NH-FR	1.81	132.2	53.7	42.7	54.3	49.8	1.26	0.99	1.08
290-D0-NH-FR	2.10	137.9	73.1	55.1	75.0	66.6	1.33	0.97	1.10
Parametric study									
240-D0-NH-T1.0	1.0	238.0	22.1	7.2	19.6	14.4	3.07	1.13	1.53
240-D0-NH-T1.5	1.5	158.0	40.4	24.3	39.4	32.4	1.66	1.03	1.25
240-D0-NH-T2.0	2.0	118.0	56.5	57.6	64.2	63.4	0.98	0.88	0.89
240-D0-NH-T2.5	2.5	94.0	86.1	89.1	93.3	93.7	0.97	0.92	0.92
290-D0-NH-T1.0	1.0	288.0	25.1	5.9	20.9	15.5	4.25	1.20	1.62
290-D0-NH-T1.5	1.5	191.3	46.2	20.1	42.2	32.1	2.30	1.09	1.44
290-D0-NH-T2.0	2.0	143.0	66.5	47.6	69.1	59.5	1.40	0.96	1.12
290-D0-NH-T2.5	2.5	114.0	90.5	92.9	100.8	99.6	0.98	0.90	0.91
Mean							1.82	1.01	1.18
COV							0.56	0.10	0.21

Table 9. Comparison of shear capacity reduction factor obtained from tests, parametric study and current design formulae for CFS channels with un-stiffened web holes (aspect ratio=1.0)

Specimen	Ratio	Shear capacity reduction factor (q_s)				Comparison		
	d_{wh}/d_1	q_s	$q_{s(AISI\&AS/NZS)}$	$q_{s(Shan)}$	$q_{s(KM)}$	$q_s/q_{s(AISI\&AS/NZS)}$	$q_s/q_{s(Shan)}$	$q_s/q_{s(KM)}$
Experiments								
240-D140-UH-FR	0.63	0.56	0.64	0.22	0.39	0.88	2.54	1.43
240-D90-UH-FR	0.42	0.84	0.81	0.30	0.66	1.04	2.80	1.25
290-D140-UH-FR	0.52	0.70	0.76	0.26	0.53	0.92	2.29	1.34
290-D90-UH-FR	0.35	0.87	0.91	0.45	0.76	0.96	1.93	1.14
Parametric study								
240-D24-UH-T1.0	0.1	1.00	NA	1.00	0.94	NA	1.00	1.06
240-D72-UH-T1.0	0.3	0.81	NA	0.61	0.81	NA	1.32	1.00
240-D120-UH-T1.0	0.5	0.53	NA	0.27	0.55	NA	1.96	0.96
240-D168-UH-T1.0	0.7	0.30	NA	0.19	0.29	NA	1.57	1.03
290-D29-UH-T1.0	0.1	1.00	NA	1.00	0.94	NA	1.00	1.06
290-D87-UH-T1.0	0.3	0.82	NA	0.61	0.82	NA	1.35	1.01
290-D145-UH-T1.0	0.5	0.58	NA	0.27	0.56	NA	2.15	1.04
290-D203-UH-T1.0	0.7	0.36	NA	0.19	0.29	NA	1.91	1.25
240-D24-UH-T1.5	0.1	0.94	1.00	1.00	0.94	0.94	0.94	1.00
240-D72-UH-T1.5	0.3	0.80	1.00	0.61	0.81	0.80	1.31	0.99
240-D120-UH-T1.5	0.5	0.52	0.94	0.27	0.55	0.55	1.93	0.95
240-D168-UH-T1.5	0.7	0.30	NA	0.19	0.29	NA	1.58	1.03
290-D29-UH-T1.5	0.1	0.97	1.00	1.00	0.94	0.97	0.97	1.03
290-D87-UH-T1.5	0.3	0.81	1.00	0.61	0.82	0.81	1.32	1.00
290-D145-UH-T1.5	0.5	0.54	1.00	0.27	0.56	0.54	2.00	0.96
290-D203-UH-T1.5	0.7	0.33	NA	0.19	0.29	NA	1.72	1.14
240-D24-UH-T2.0	0.1	1.00	1.00	1.00	0.94	1.00	1.00	1.06
240-D72-UH-T2.0	0.3	0.86	0.85	0.61	0.81	1.01	1.41	1.06
240-D120-UH-T2.0	0.5	0.57	0.69	0.27	0.55	0.81	2.07	1.02
240-D168-UH-T2.0	0.7	0.35	NA	0.19	0.29	NA	1.79	1.17
290-D29-UH-T2.0	0.1	1.00	1.00	1.00	0.94	1.00	1.00	1.06
290-D87-UH-T2.0	0.3	0.86	1.00	0.61	0.82	0.86	1.41	1.05
290-D145-UH-T2.0	0.5	0.56	0.84	0.27	0.56	0.67	2.07	1.00
290-D203-UH-T2.0	0.7	0.34	NA	0.19	0.29	NA	1.79	1.17
240-D24-UH-T2.5	0.1	0.99	0.81	1.00	0.94	1.22	1.00	1.06
240-D72-UH-T2.5	0.3	0.80	0.68	0.61	0.81	1.18	1.31	0.99
240-D120-UH-T2.5	0.5	0.53	0.55	0.27	0.55	0.96	1.96	0.96
240-D168-UH-T2.5	0.7	0.31	NA	0.19	0.29	NA	1.63	1.07
290-D29-UH-T2.5	0.1	0.99	0.98	1.00	0.94	1.01	0.99	1.06
290-D87-UH-T2.5	0.3	0.82	0.82	0.61	0.82	1.00	1.34	1.00
290-D145-UH-T2.5	0.5	0.58	0.67	0.27	0.56	0.85	2.11	1.02
290-D203-UH-T2.5	0.7	0.36	NA	0.19	0.29	NA	1.89	1.24
Mean						0.91	1.62	1.07
COV						0.18	0.29	0.10

NA: h/t_w ratio or d_{wh} exceeds the limit of AS/NZS (2018)

Table 10. Comparison of shear capacity reduction factor obtained from tests, parametric study, current design formulae and proposed design formulae for channels with edge-stiffened web holes (aspect ratio=1.0)

Specimen	Ratio	Shear capacity reduction factor (q_s)					Comparison			
	d_{wh}/d_1	q_s	$q_{s(AISI\&AS/NZS)}$	$q_{s(Shan)}$	$q_{s(KM)}$	$q_{s(pr)}$	$q_s/q_{s(AISI\&AS/NZS)}$	$q_s/q_{s(Shan)}$	$q_s/q_{s(KM)}$	$q_s/q_{s(pr)}$
Experiments										
240-D140-EH	0.63	0.66	0.64	0.22	0.39	0.59	1.03	3.00	1.69	1.12
240-D90-EH	0.41	0.91	0.81	0.30	0.66	0.83	1.12	3.03	1.38	1.10
290-D140-EH	0.52	0.76	0.76	0.26	0.53	0.79	1.00	2.92	1.43	0.96
290-D90-EH	0.34	0.88	0.91	0.45	0.76	0.93	0.97	1.96	1.16	0.95
Parametric study										
240-D24-EH-T1.5-Q0.04	0.1	1.00	1.00	1.00	0.94	1.01	1.00	1.00	1.06	0.99
240-D72-EH-T1.5-Q0.04	0.3	0.88	1.00	0.61	0.81	0.89	0.88	1.44	1.09	0.99
240-D120-EH-T1.5-Q0.04	0.5	0.67	0.94	0.27	0.55	0.67	0.71	2.48	1.22	1.00
240-D168-EH-T1.5-Q0.04	0.7	0.45	NA	0.19	0.29	0.43	NA	2.37	1.55	1.05
240-D24-EH-T1.5-Q0.06	0.1	1.00	1.00	1.00	0.94	1.02	1.00	1.00	1.06	0.98

240-D72-EH-T1.5-Q0.06	0.3	0.89	1.00	0.61	0.81	0.90	0.89	1.46	1.10	0.99
240-D120-EH-T1.5-Q0.06	0.5	0.69	0.94	0.27	0.55	0.69	0.73	2.56	1.25	1.00
240-D168-EH-T1.5-Q0.06	0.7	0.46	NA	0.19	0.29	0.45	NA	2.42	1.59	1.02
240-D24-EH-T2.0-Q0.04	0.1	1.01	1.00	1.00	0.94	1.01	1.01	1.01	1.07	1.00
240-D72-EH-T2.0-Q0.04	0.3	0.87	0.85	0.61	0.81	0.89	1.02	1.43	1.07	0.98
240-D120-EH-T2.0-Q0.04	0.5	0.70	0.79	0.27	0.55	0.67	0.89	2.59	1.27	1.04
240-D168-EH-T2.0-Q0.04	0.7	0.45	NA	0.19	0.29	0.43	NA	2.37	1.55	1.05
240-D24-EH-T2.0-Q0.06	0.1	1.01	1.00	1.00	0.94	1.02	1.01	1.01	1.07	0.99
240-D72-EH-T2.0-Q0.06	0.3	0.88	0.85	0.61	0.81	0.90	1.04	1.44	1.09	0.98
240-D120-EH-T2.0-Q0.06	0.5	0.72	0.79	0.27	0.55	0.69	0.91	2.67	1.31	1.04
240-D168-EH-T2.0-Q0.06	0.7	0.47	NA	0.19	0.29	0.45	NA	2.47	1.62	1.04
290-D29-EH-T1.5-Q0.04	0.1	1.01	1.00	1.00	0.94	1.01	1.01	1.01	1.07	1.00
290-D87-EH-T1.5-Q0.04	0.3	0.91	1.00	0.61	0.81	0.89	0.91	1.49	1.12	1.02
290-D145-EH-T1.5-Q0.04	0.5	0.64	1.00	0.27	0.55	0.67	0.64	2.37	1.16	0.96
290-D203-EH-T1.5-Q0.04	0.7	0.44	NA	0.19	0.29	0.43	NA	2.32	1.52	1.02
290-D29-EH-T1.5-Q0.06	0.1	1.02	1.00	1.00	0.94	1.02	1.02	1.02	1.09	1.00
290-D87-EH-T1.5-Q0.06	0.3	0.92	1.00	0.61	0.81	0.90	0.92	1.51	1.14	1.02
290-D145-EH-T1.5-Q0.06	0.5	0.67	1.00	0.27	0.55	0.69	0.67	2.48	1.22	0.97
290-D203-EH-T1.5-Q0.06	0.7	0.47	NA	0.19	0.29	0.45	NA	2.47	1.62	1.04
290-D29-EH-T2.0-Q0.04	0.1	1.01	1.00	1.00	0.94	1.01	1.01	1.01	1.07	1.00
290-D87-EH-T2.0-Q0.04	0.3	0.91	1.00	0.61	0.81	0.89	0.91	1.49	1.12	1.02
290-D145-EH-T2.0-Q0.04	0.5	0.68	0.84	0.27	0.55	0.67	0.81	2.52	1.24	1.01
290-D203-EH-T2.0-Q0.04	0.7	0.44	NA	0.19	0.29	0.43	NA	2.32	1.52	1.02
290-D29-EH-T2.0-Q0.06	0.1	1.02	1.00	1.00	0.94	1.02	1.02	1.02	1.09	1.00
290-D87-EH-T2.0-Q0.06	0.3	0.93	1.00	0.61	0.81	0.90	0.93	1.52	1.15	1.03
290-D145-EH-T2.0-Q0.06	0.5	0.71	0.84	0.27	0.55	0.69	0.85	2.63	1.29	1.03
290-D203-EH-T2.0-Q0.06	0.7	0.47	NA	0.19	0.29	0.45	NA	2.47	1.62	1.04
Mean							0.93	1.95	1.27	1.01
COV							0.13	0.35	0.16	0.03

Table 11. Statistical parameters for comparison of shear capacity reduction factor obtained from tests and parametric study against the proposed design formulae

(a) $0.1 \le d_{wh}/d_1 \le 0.3$

Statistical parameters	$q_{s(FEA\&TEST)} / q_{s(pr)} = 1.04 + 0.67\frac{q}{d_1} - 0.59\frac{d_{wh}}{d_1}$
Number of data	80
Mean, P_m	1.00
Coefficient of variation, COV	0.02
Reliability index, β	2.84
Resistance factor, φ	0.85

(b) $0.3 < d_{wh}/d_1 \le 0.5$

Statistical parameters	$q_{s(FEA\&TEST)} / q_{s(pr)} = 1.42 + 1.08\frac{q}{d_1} - 1.59\frac{d_{wh}}{d_1}$
Number of data	42
Mean, P_m	1.00
Coefficient of variation, COV	0.04
Reliability index, β	2.80
Resistance factor, φ	0.85

(c) $0.5 < d_{wh}/d_1 \le 0.7$

Statistical parameters	$q_{s(FEA\&TEST)} / q_{s(pr)} = 1.72 + 1.18\frac{q}{d_1} - 1.91\frac{d_{wh}}{d_1}$
Number of data	42
Mean, P_m	1.00
Coefficient of variation, COV	0.04
Reliability index, β	2.80
Resistance factor, φ	0.85

Click here to access/download;Figure;Fig.1.bmp

Click here to access/download;Figure;Fig.2(a).bmp

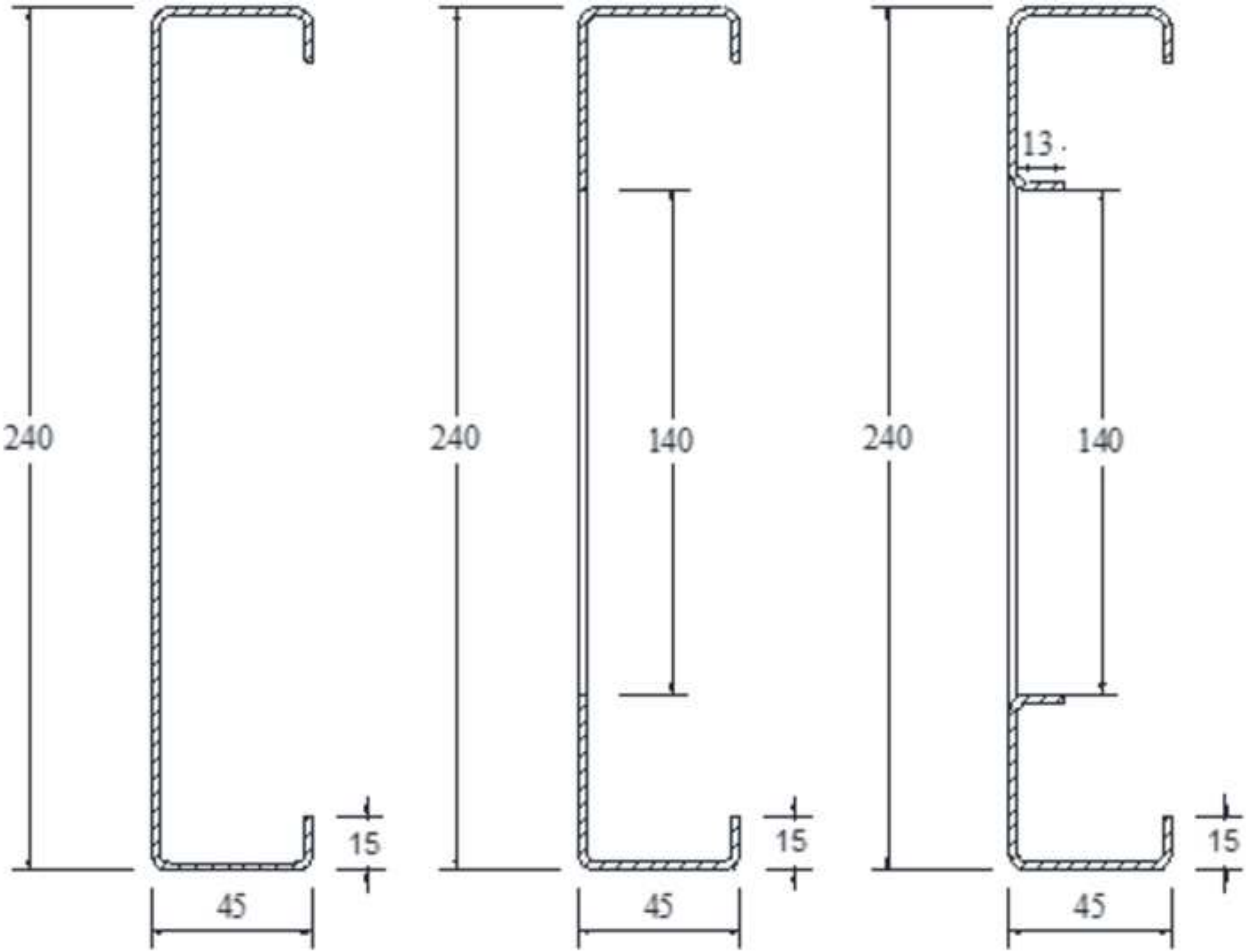

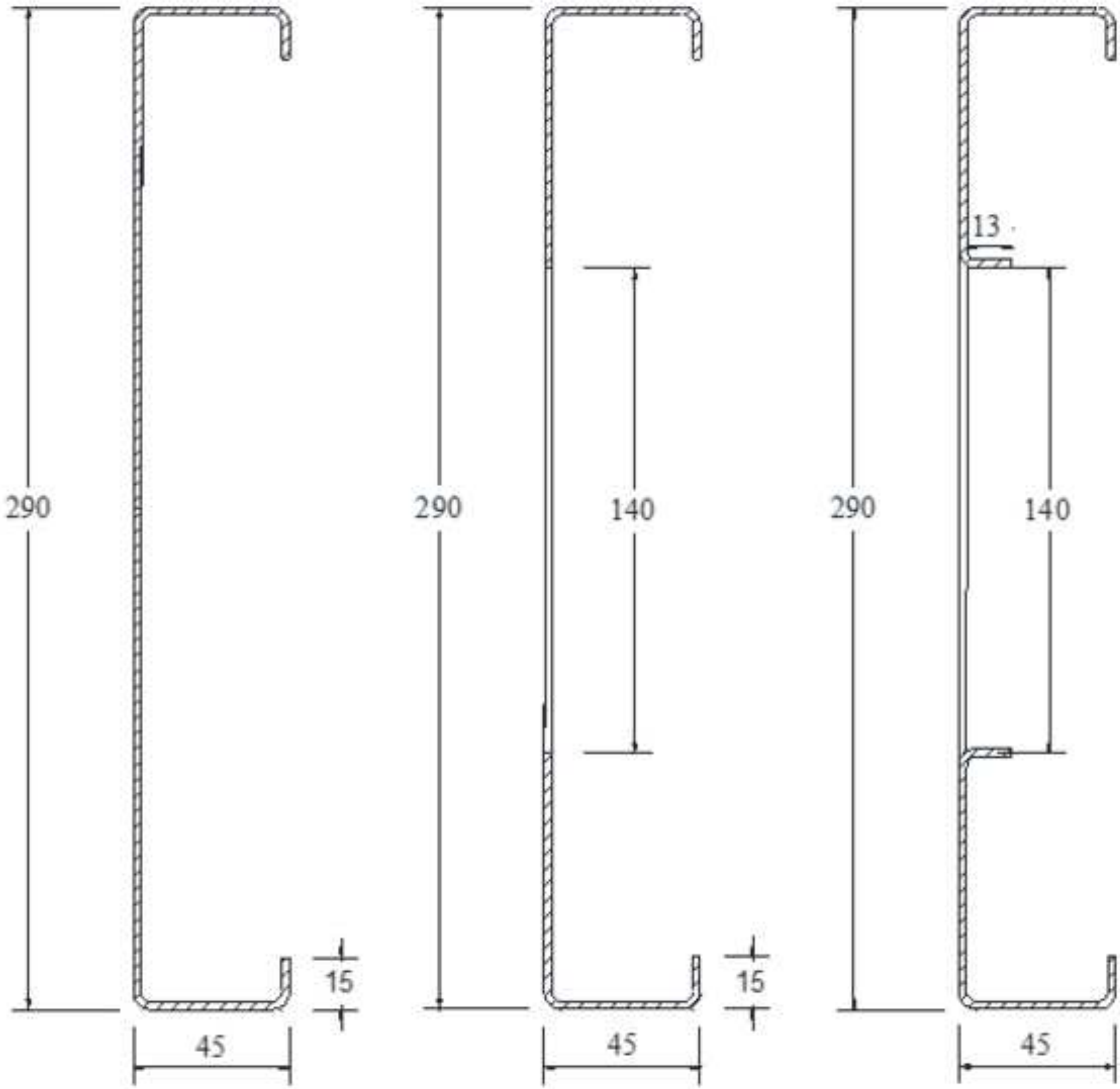
290
45
15
290
140
45
15
290
13
140
45

Click here to access/download;Figure;Fig.3(b).bmp

Click here to access/download;Figure;Fig.3(c).bmp

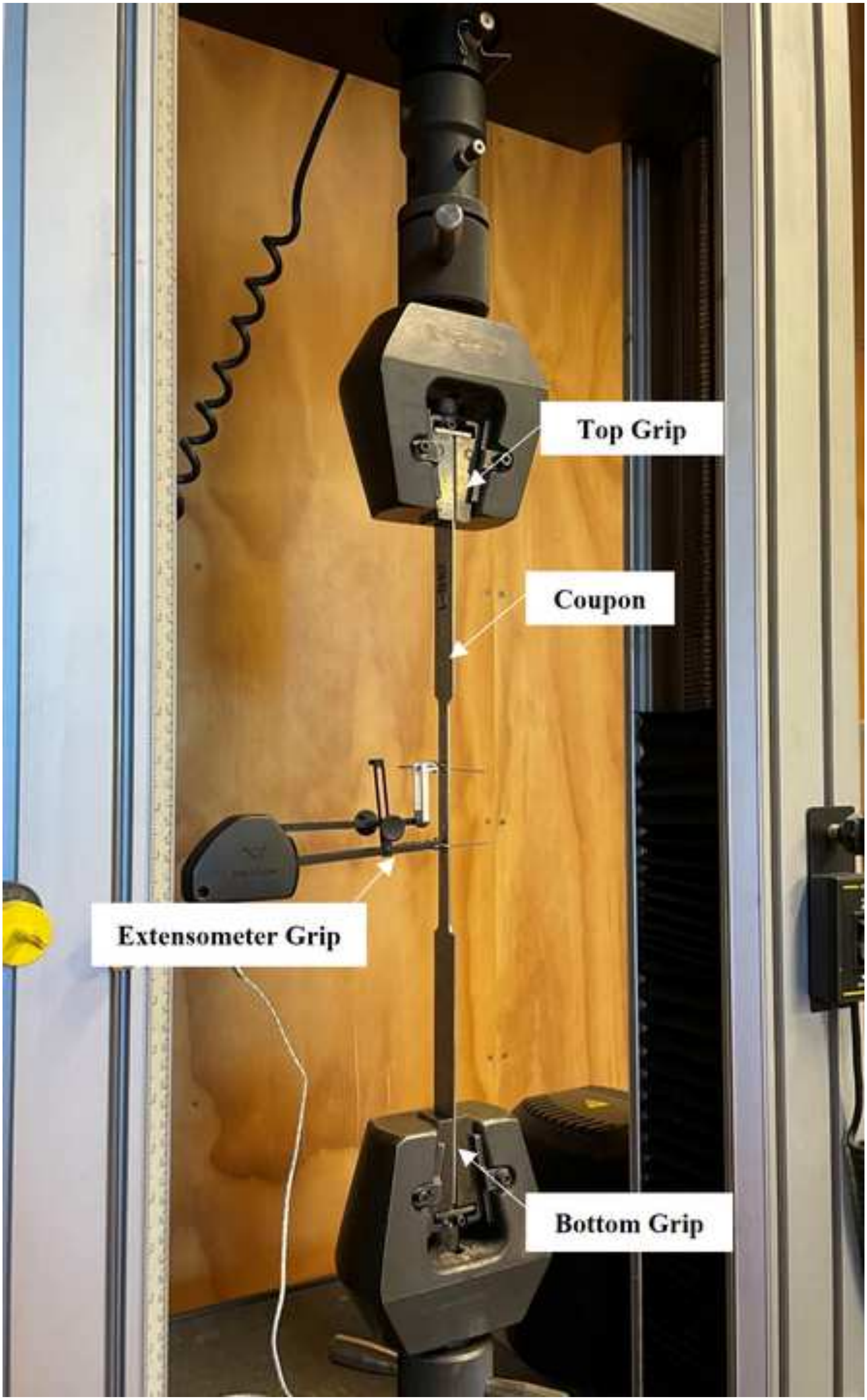
Top Grip
Coupon
Extensometer Grip
Bottom Grip

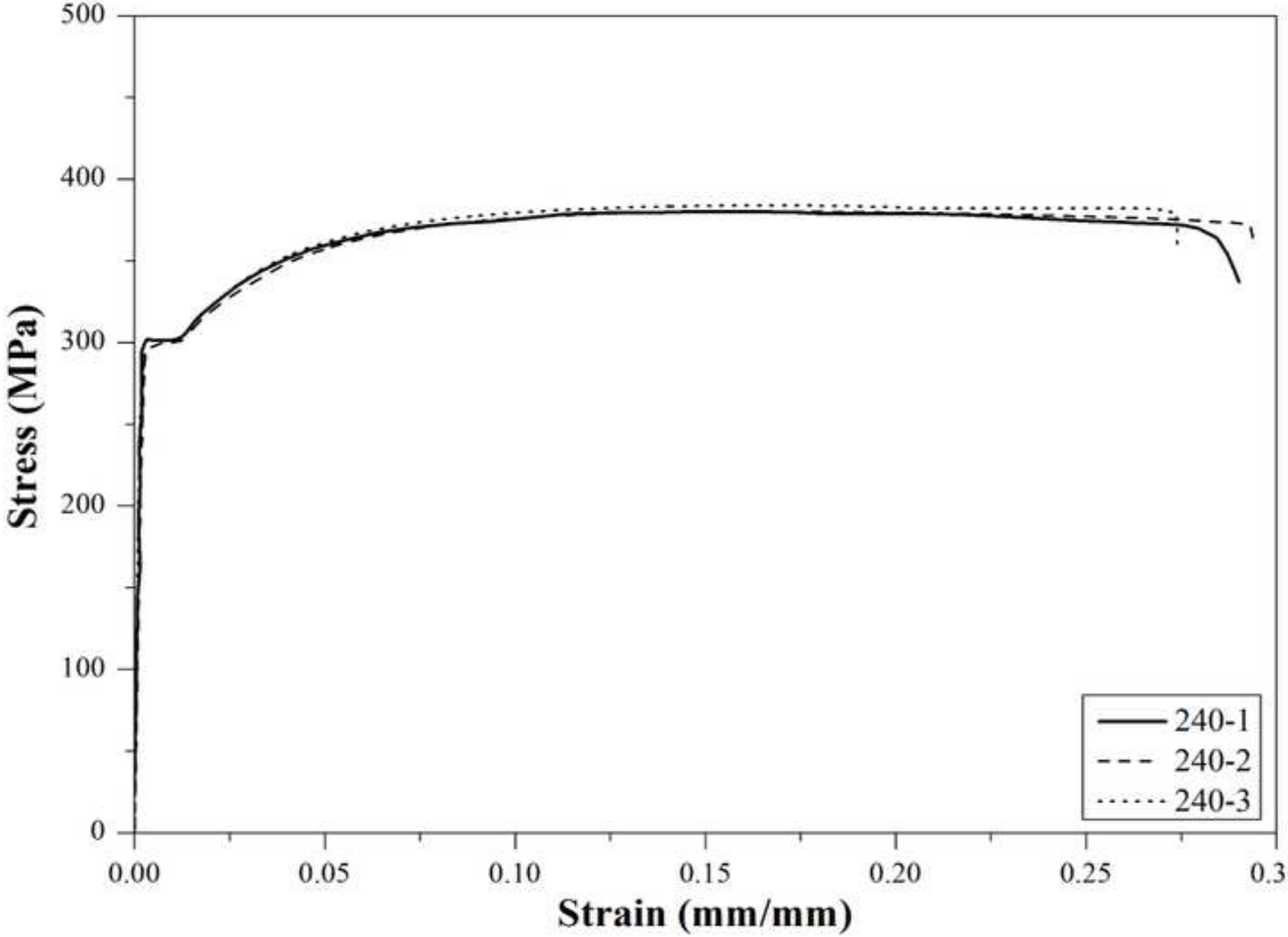
500
400
300
200
100
0
Stress (MPa)
0.00
0.05
0.10
0.15
0.20
0.25
0.3
Strain (mm/mm)
240-1
240-2
240-3

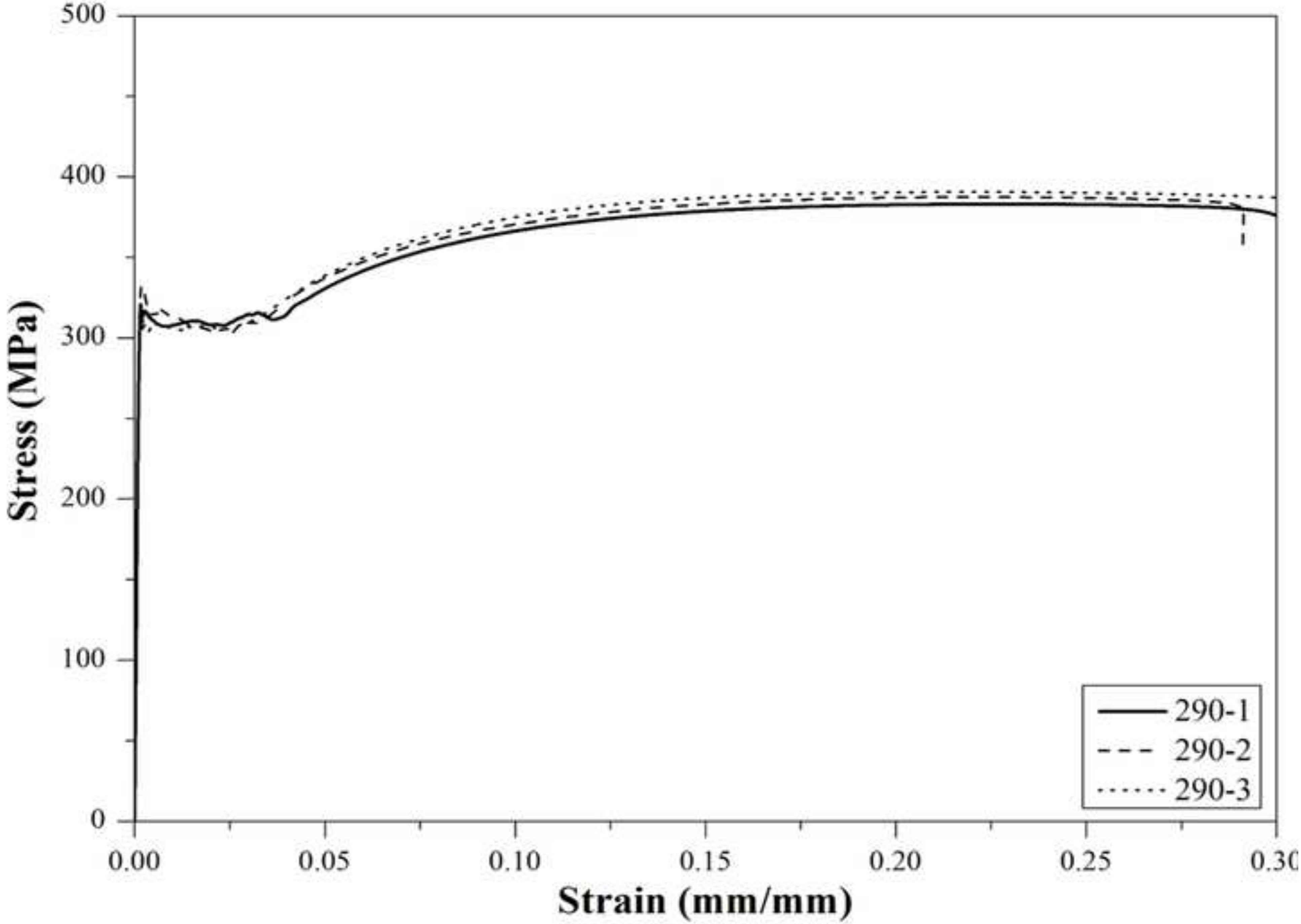

500
400
300
200
100
0
Stress (MPa)
0.00
0.05
0.10
0.15
0.20
0.25
0.30
Strain (mm/mm)
290-1
290-2
290-3

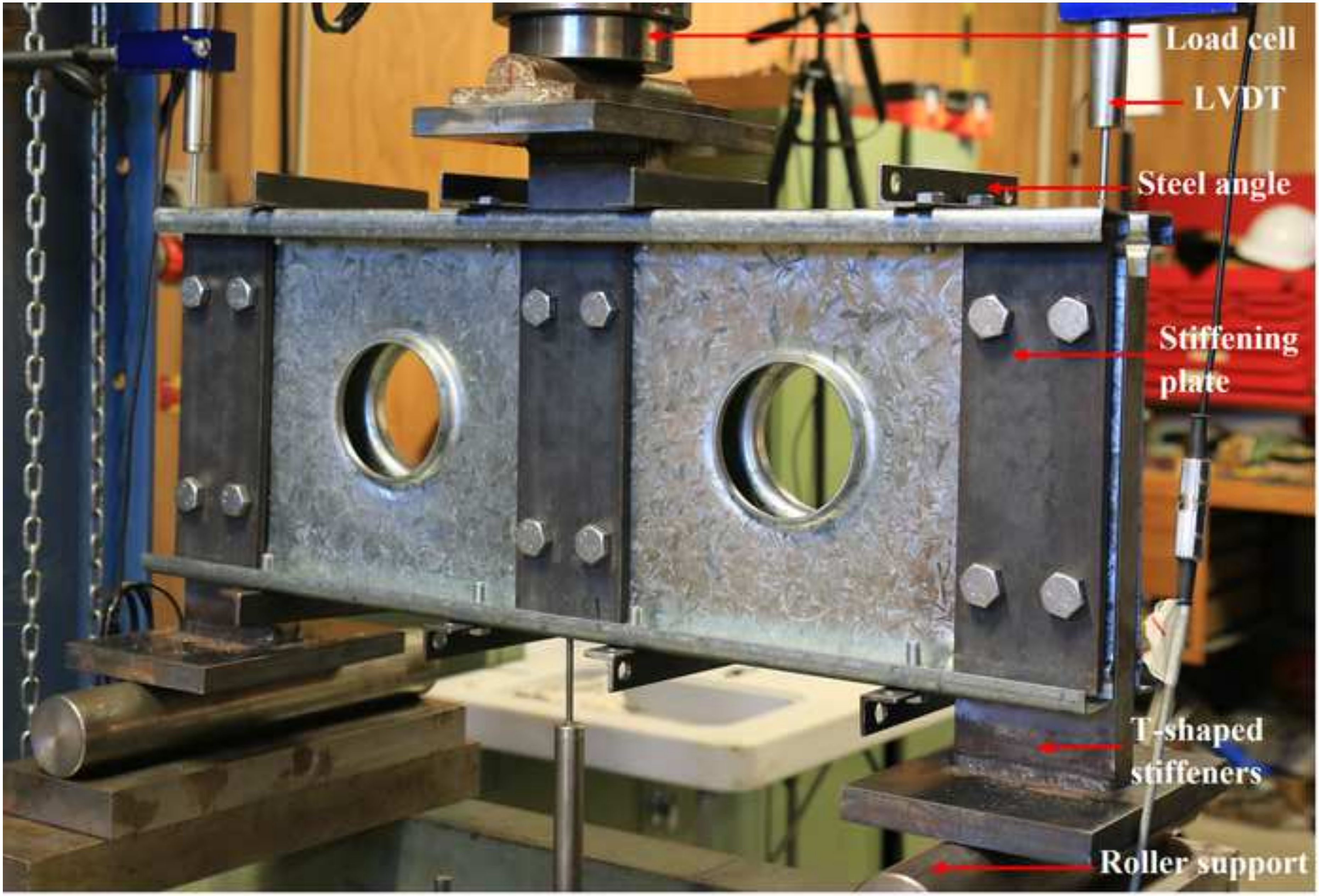
Load cell
LVDT
Steel angle
Stiffening plate
T-shaped stiffeners
Roller support

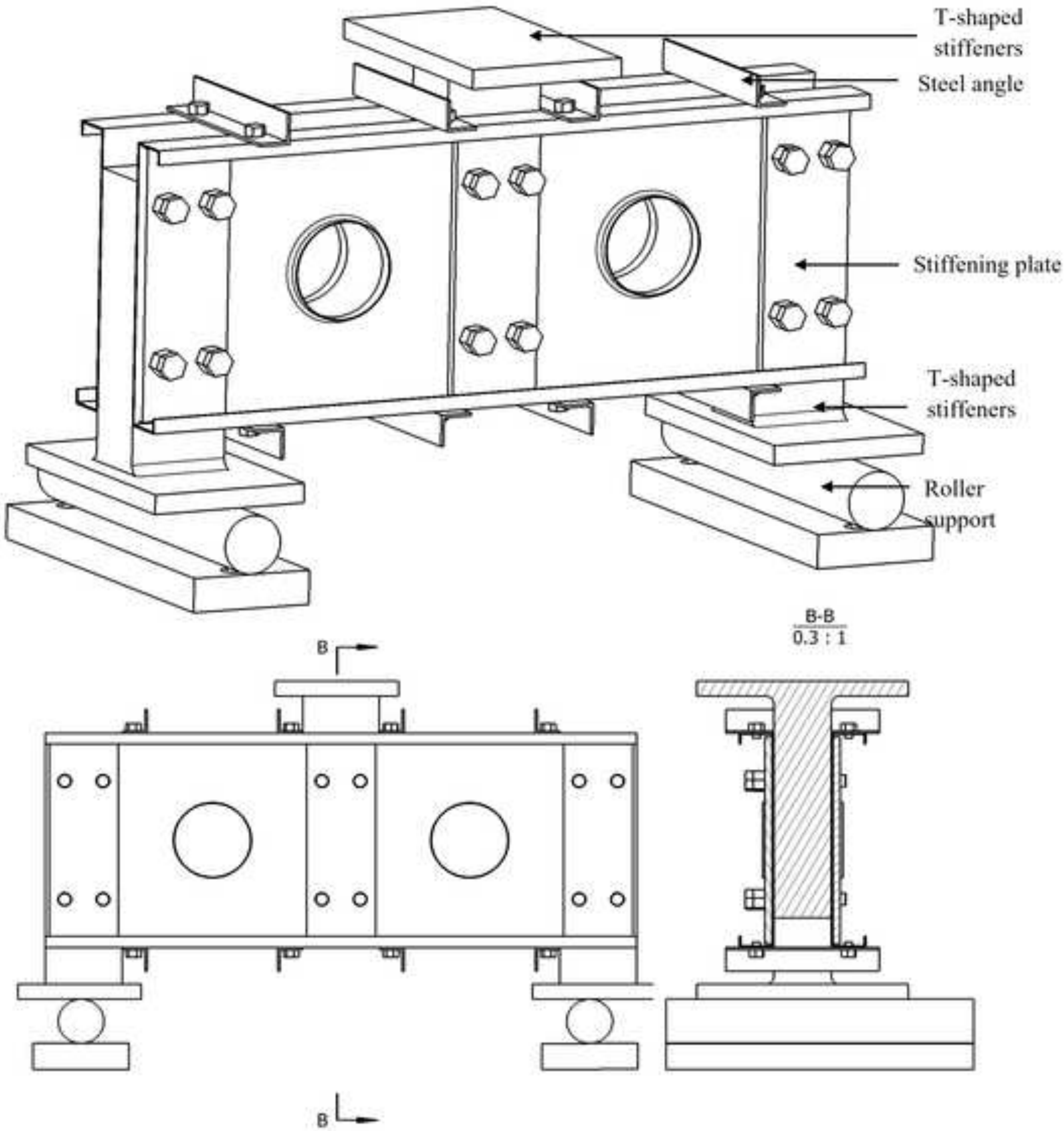
T-shaped stiffeners
Steel angle
Stiffening plate
T-shaped stiffeners
Roller support
B-B
0.3 : 1
B
B

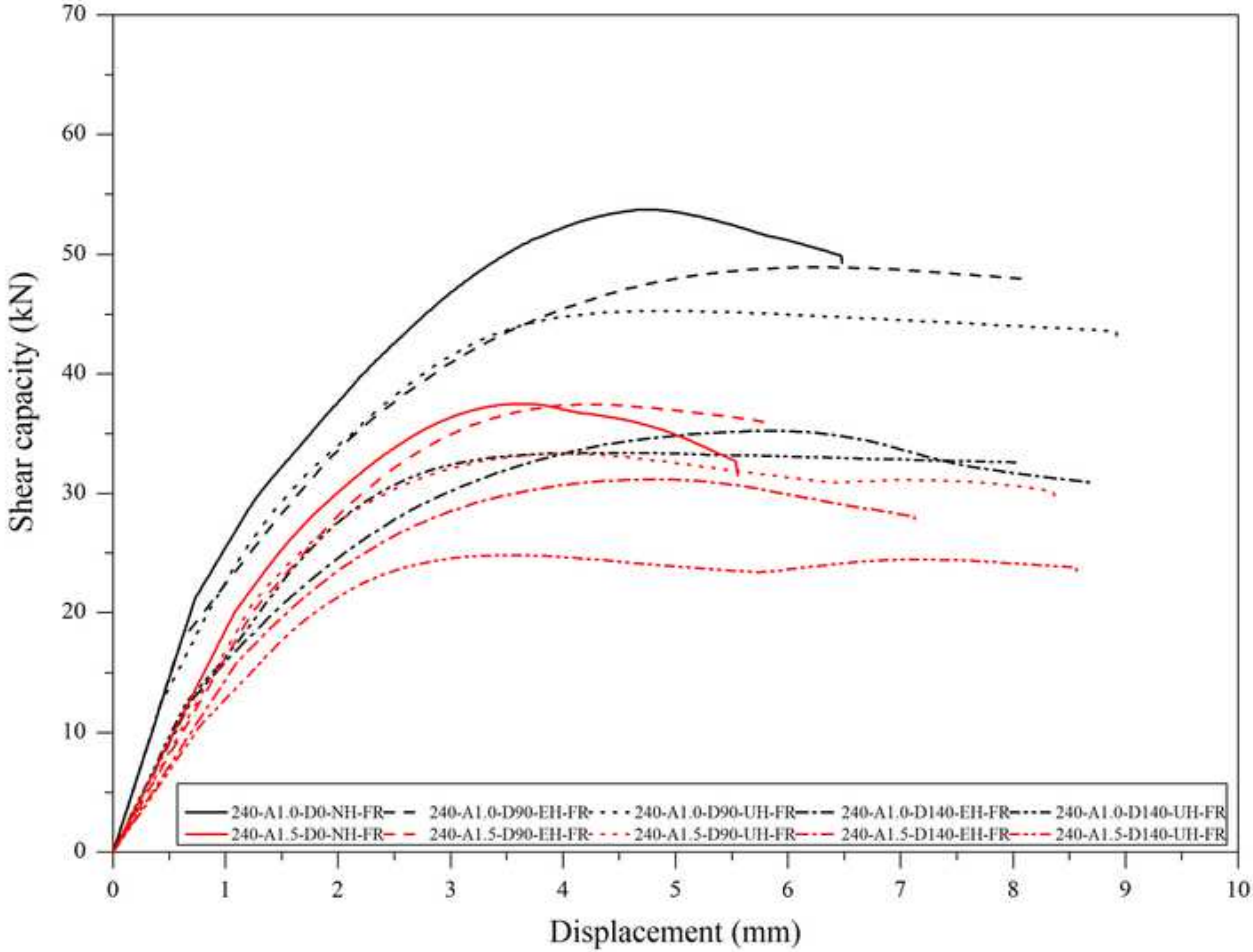

Shear capacity (kN)
Displacement (mm)
0
10
20
30
40
50
60
70
0
1
2
3
4
5
6
7
8
9
10
240-A1.0-D0-NH-FR
240-A1.0-D90-EH-FR
240-A1.0-D90-UH-FR
240-A1.0-D140-EH-FR
240-A1.0-D140-UH-FR
240-A1.5-D0-NH-FR
240-A1.5-D90-EH-FR
240-A1.5-D90-UH-FR
240-A1.5-D140-EH-FR
240-A1.5-D140-UH-FR

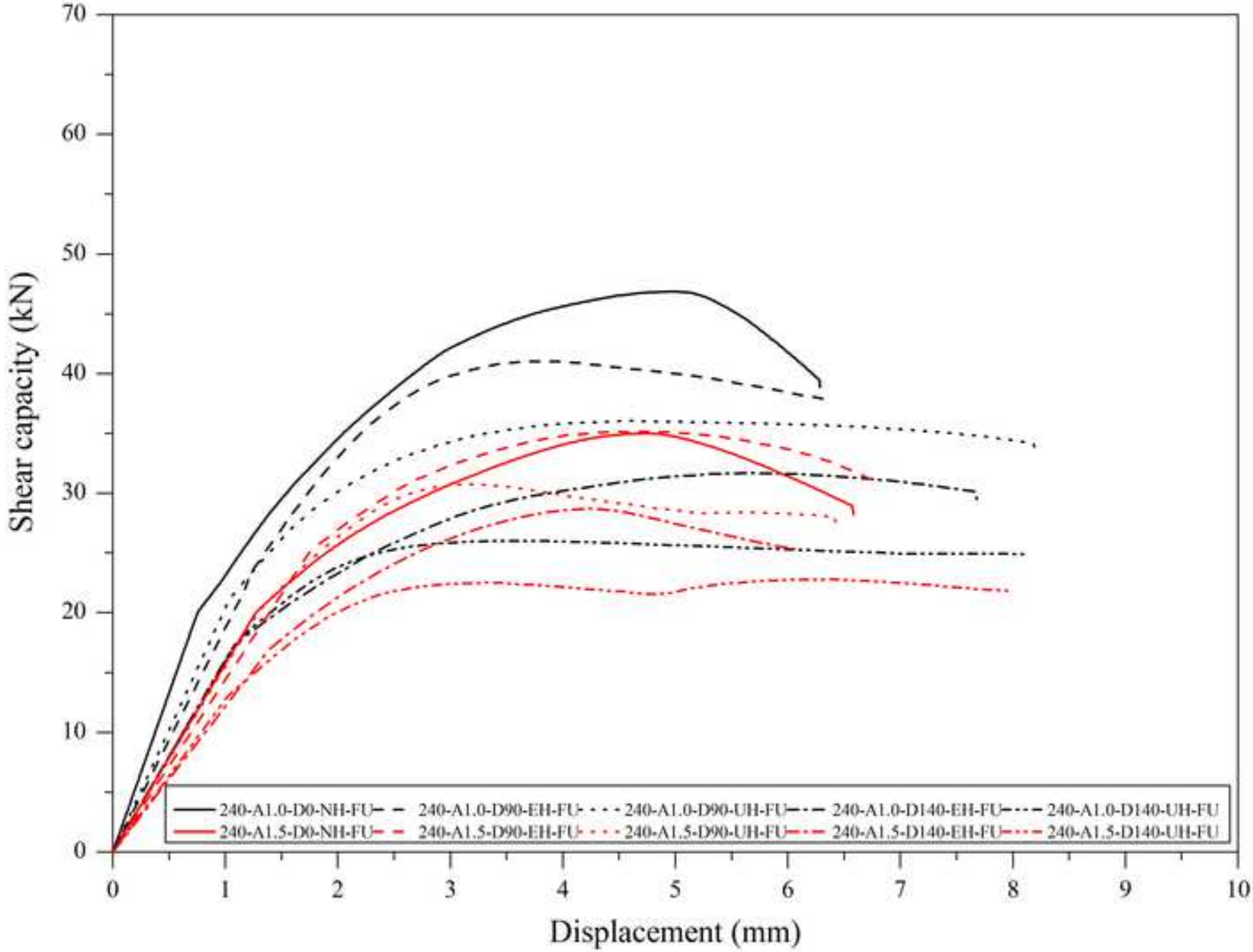
Shear capacity (kN)
Displacement (mm)
0
10
20
30
40
50
60
70
0
1
2
3
4
5
6
7
8
9
10
240-A1.0-D0-NH-FU
240-A1.0-D90-EH-FU
240-A1.0-D90-UH-FU
240-A1.0-D140-EH-FU
240-A1.0-D140-UH-FU
240-A1.5-D0-NH-FU
240-A1.5-D90-EH-FU
240-A1.5-D90-UH-FU
240-A1.5-D140-EH-FU
240-A1.5-D140-UH-FU

Click here to access/download;Figure;Fig.8(c).bmp

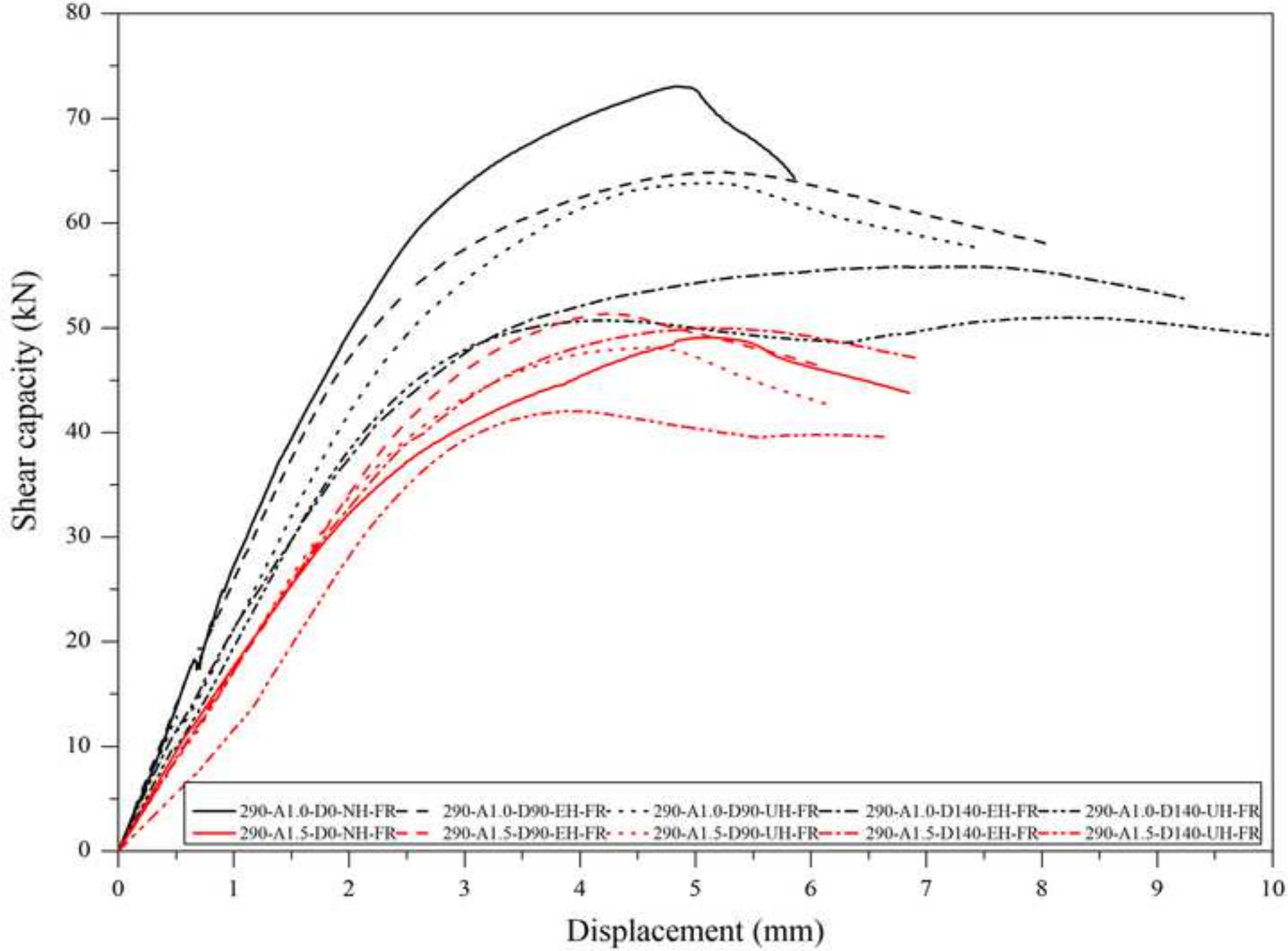

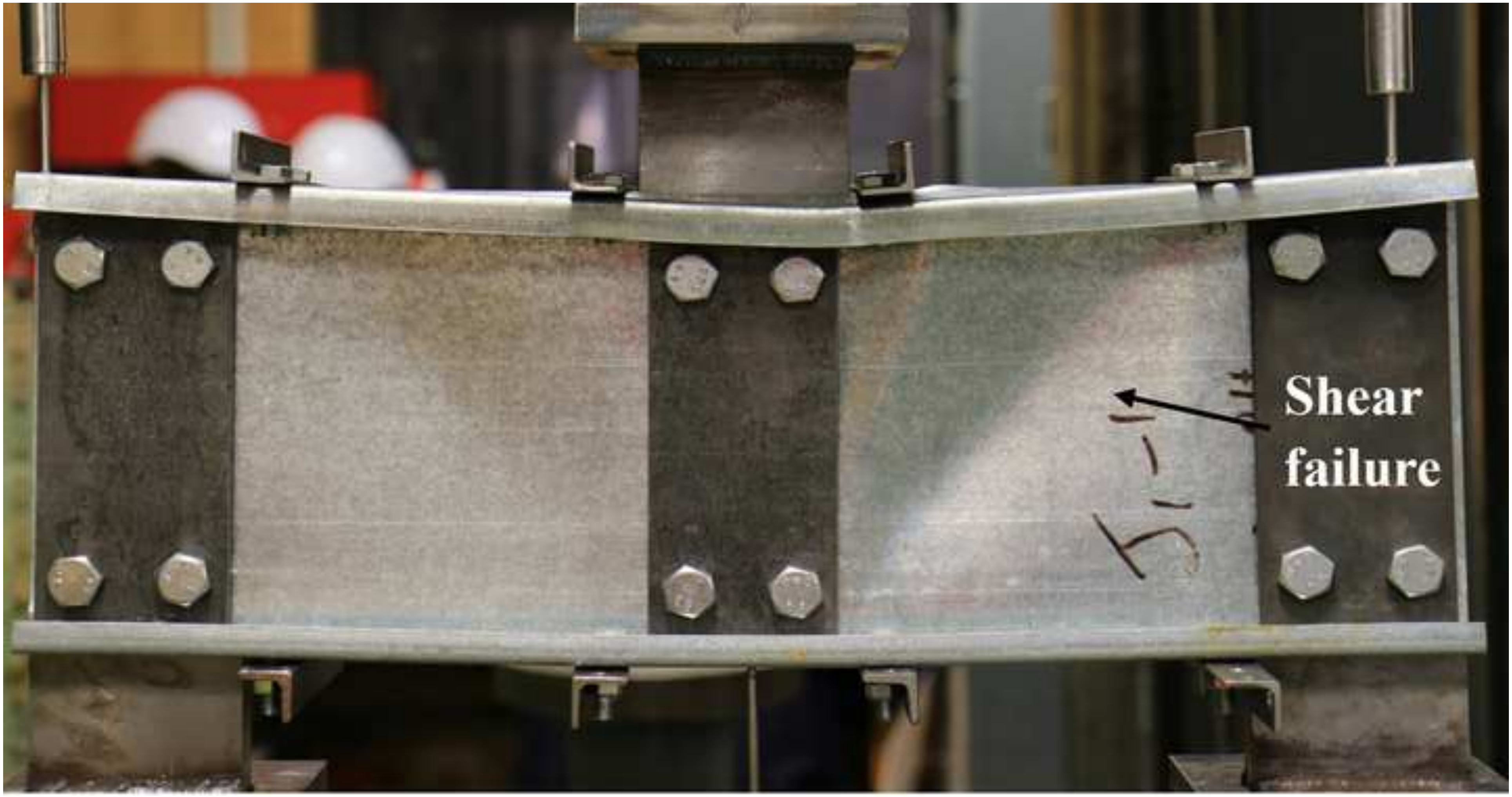
Shear
failure

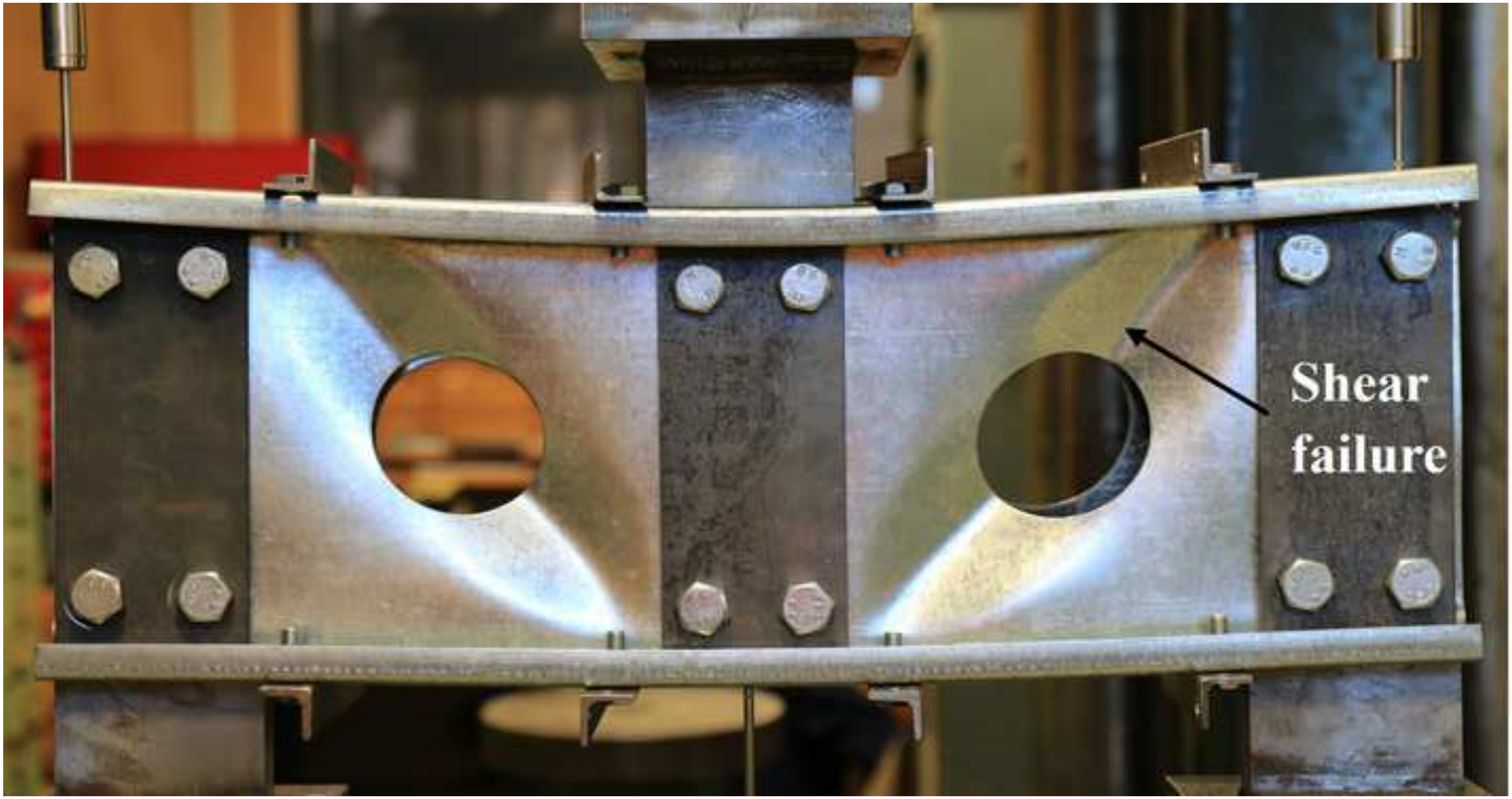
Shear
failure


Shear
failure

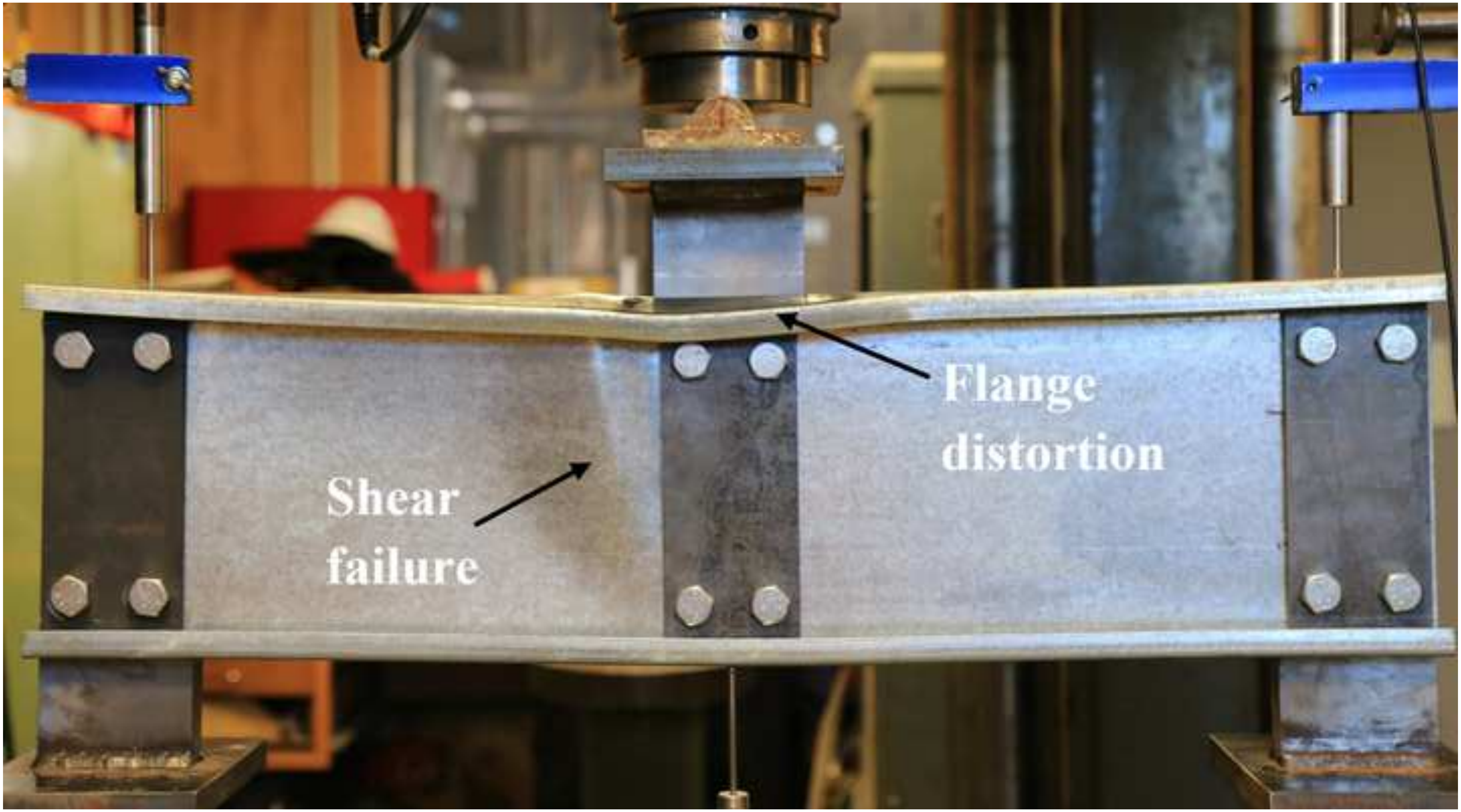
Flange
distortion
Shear
failure

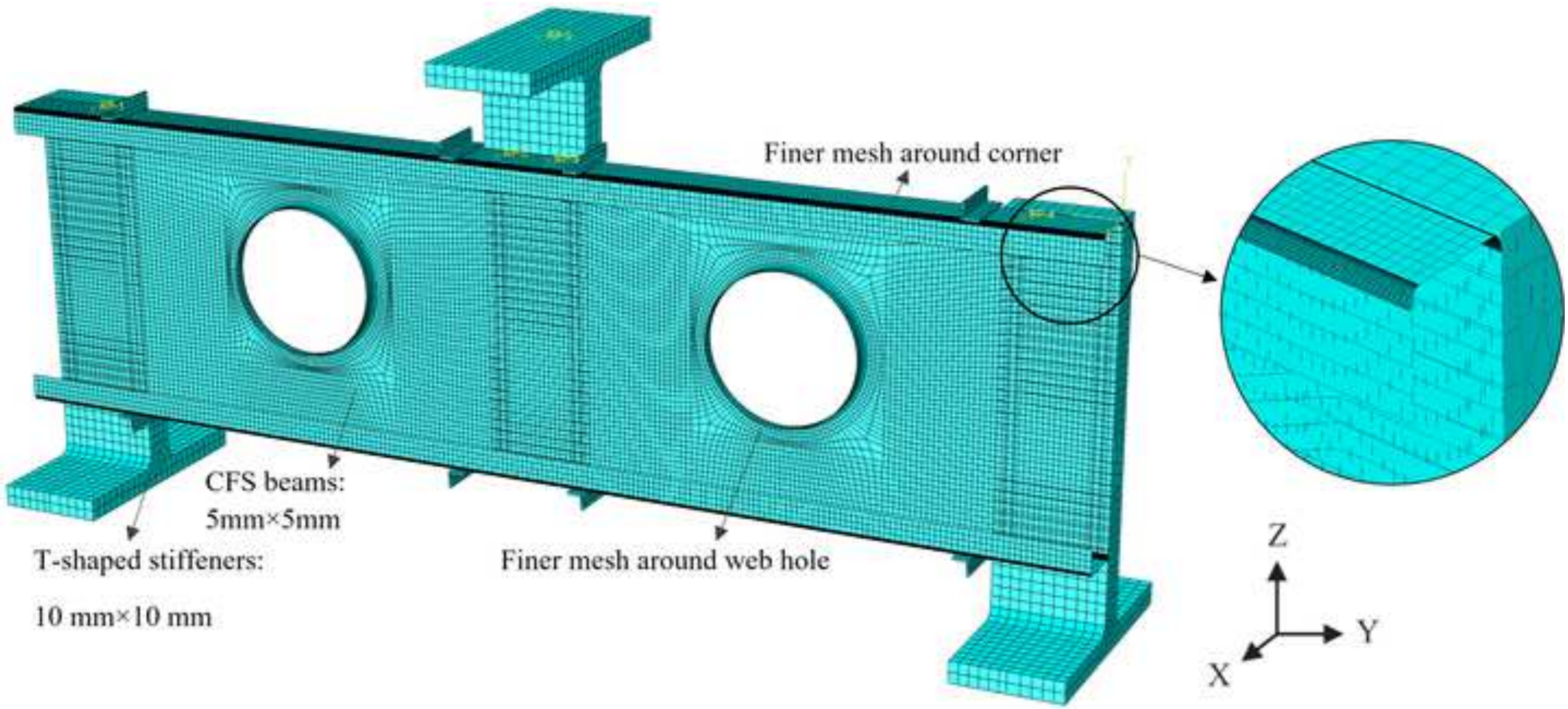
Finer mesh around corner
CFS beams:
5mm×5mm
T-shaped stiffeners:
10 mm×10 mm
Finer mesh around web hole
Z
Y
X

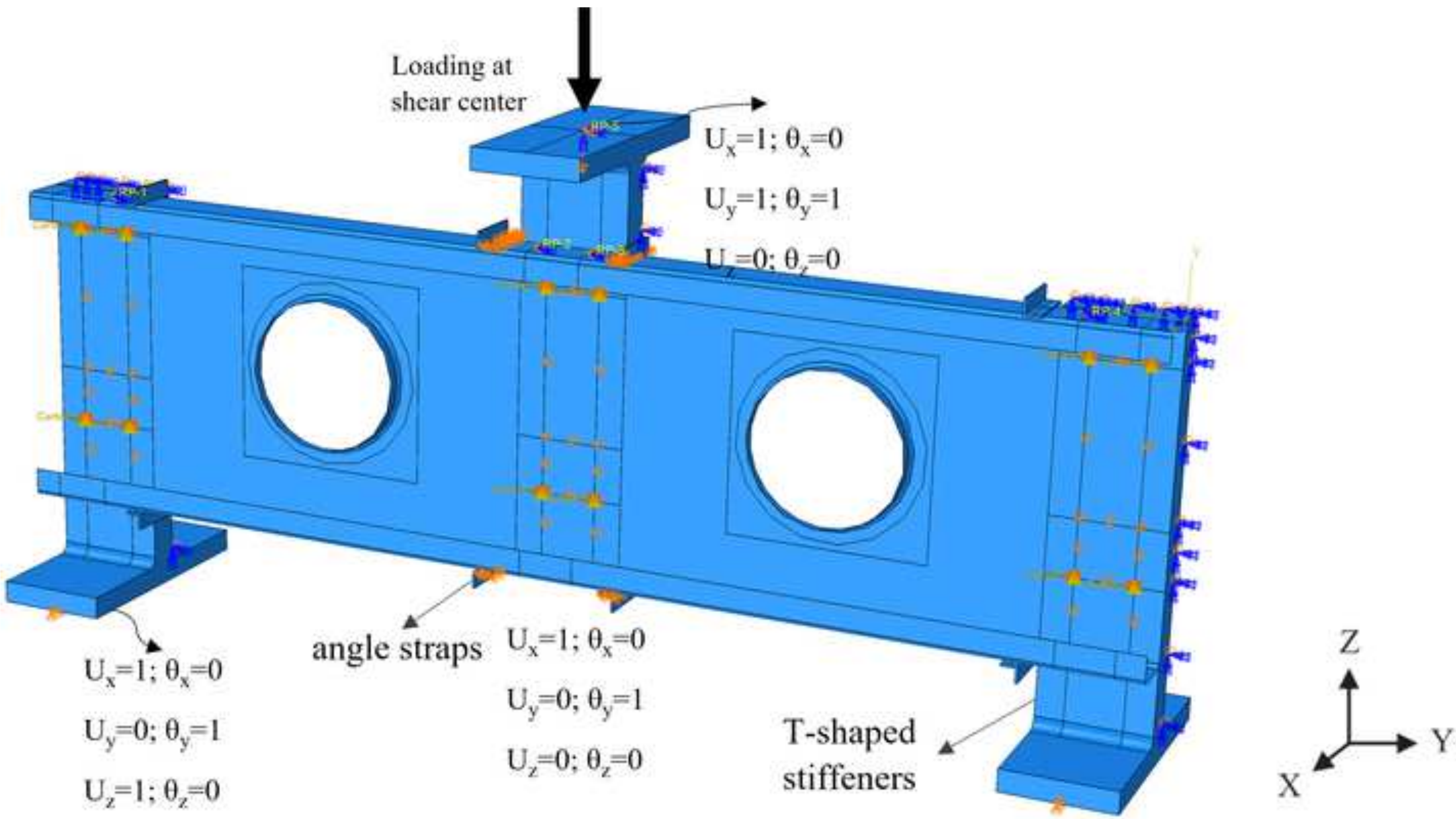

Loading at
shear center
U_x=1; θ_x=0
U_y=1; θ_y=1
U_z=0; θ_z=0
angle straps
U_x=1; θ_x=0
U_y=0; θ_y=1
U_z=1; θ_z=0
U_x=1; θ_x=0
U_y=0; θ_y=1
U_z=0; θ_z=0
T-shaped
stiffeners
Z
Y
X

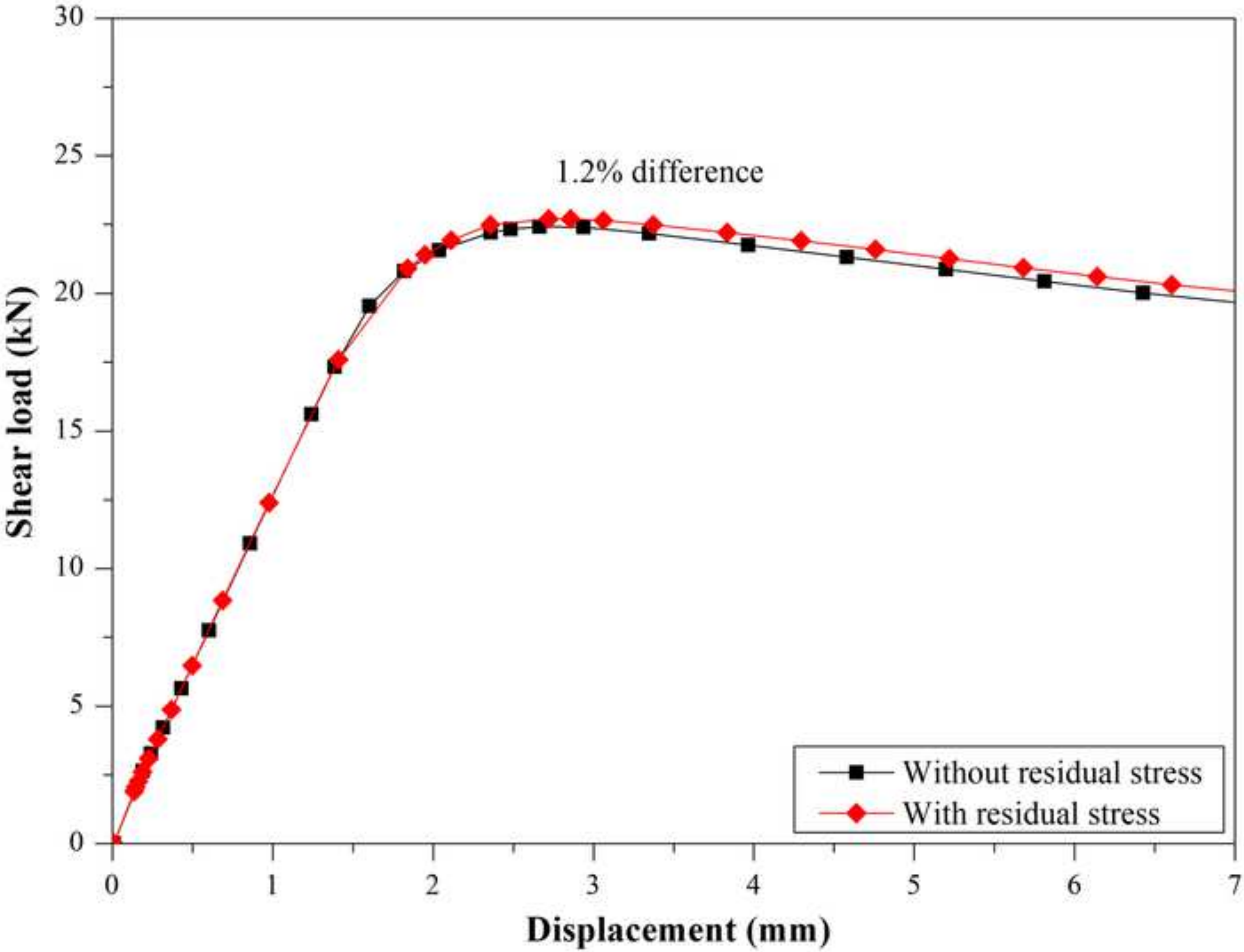
1.2% difference
Shear load (kN)
Displacement (mm)
0
5
10
15
20
25
30
0
1
2
3
4
5
6
7
Without residual stress
With residual stress

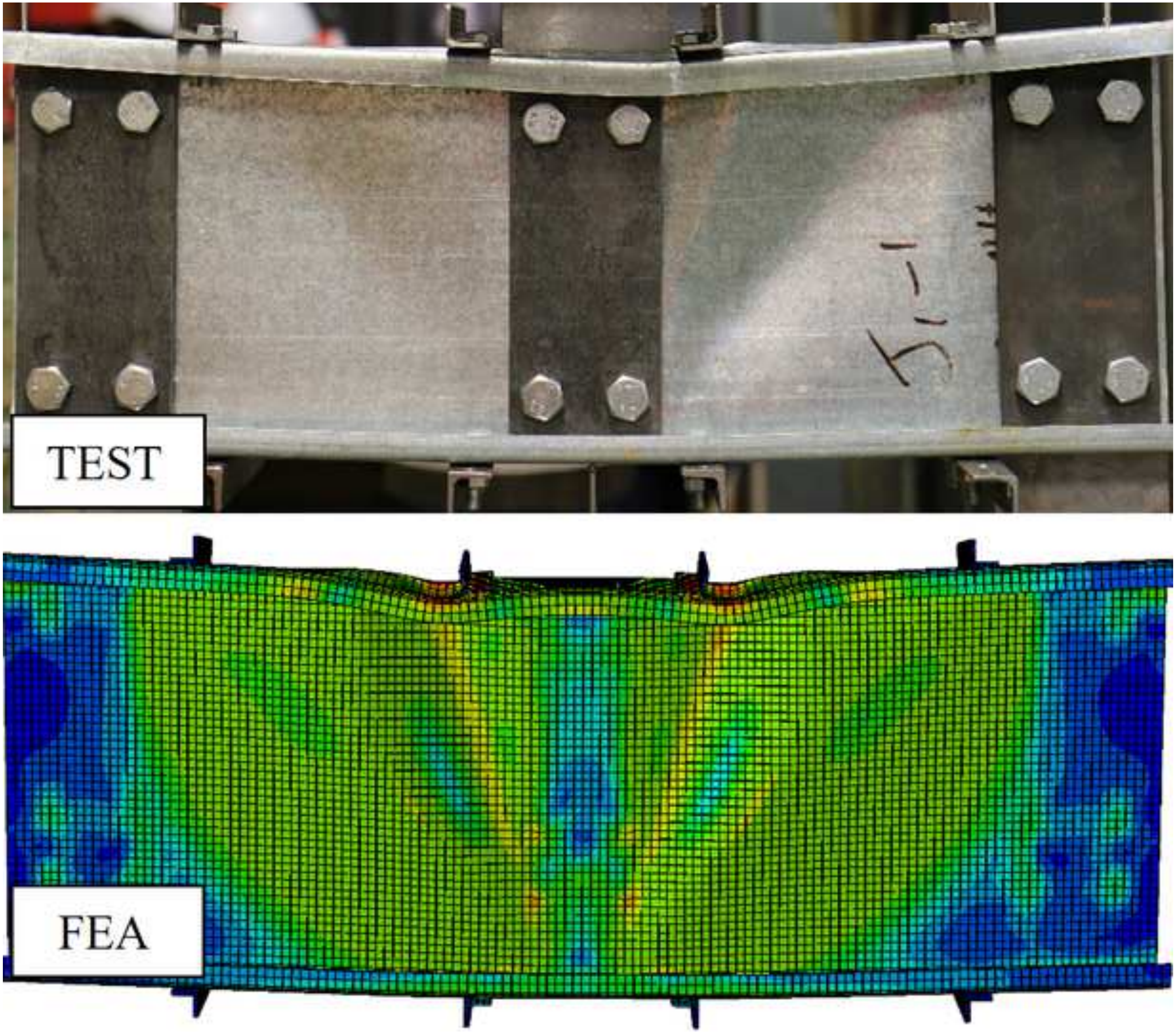
TEST
FEA

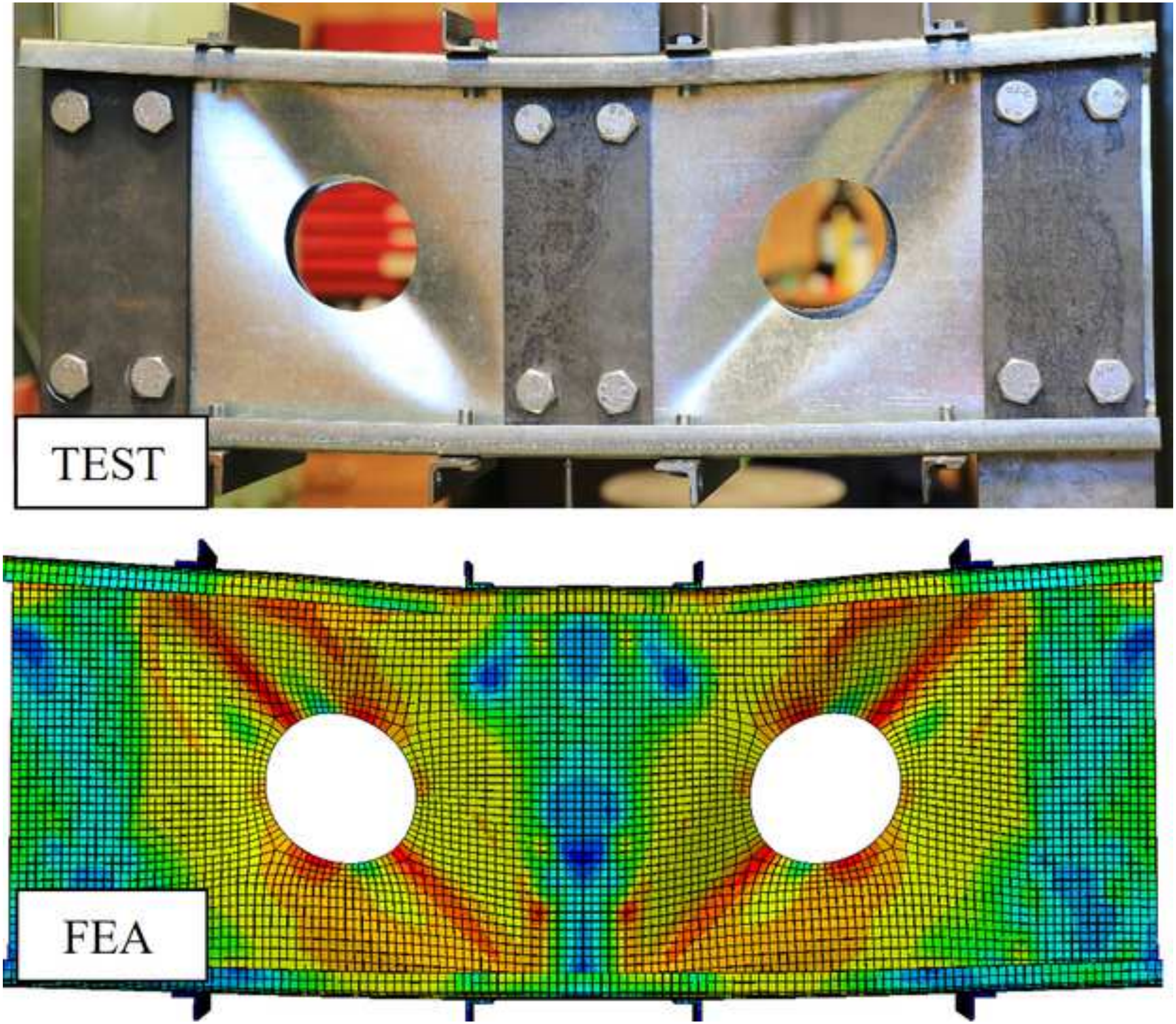
TEST
FEA

Click here to access/download;Figure;Fig.14(c).bmp

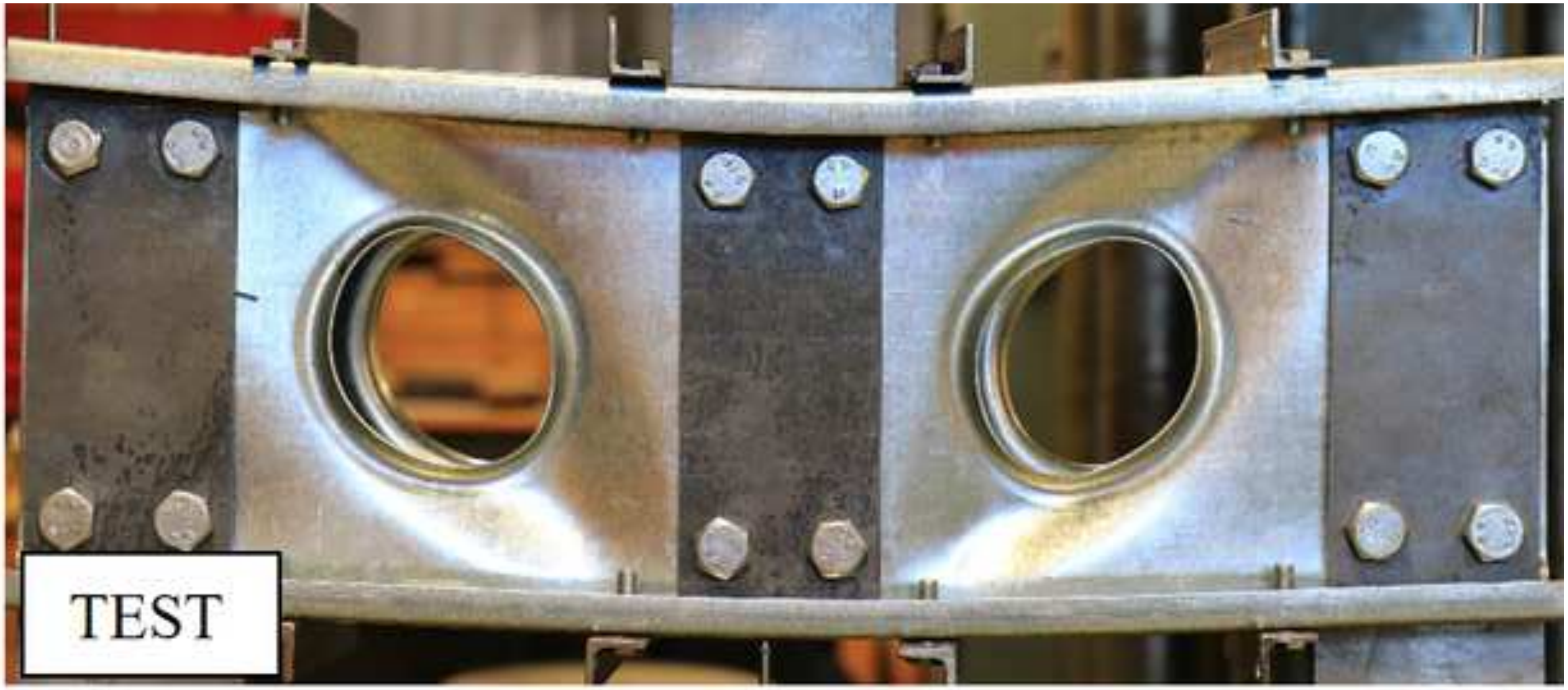

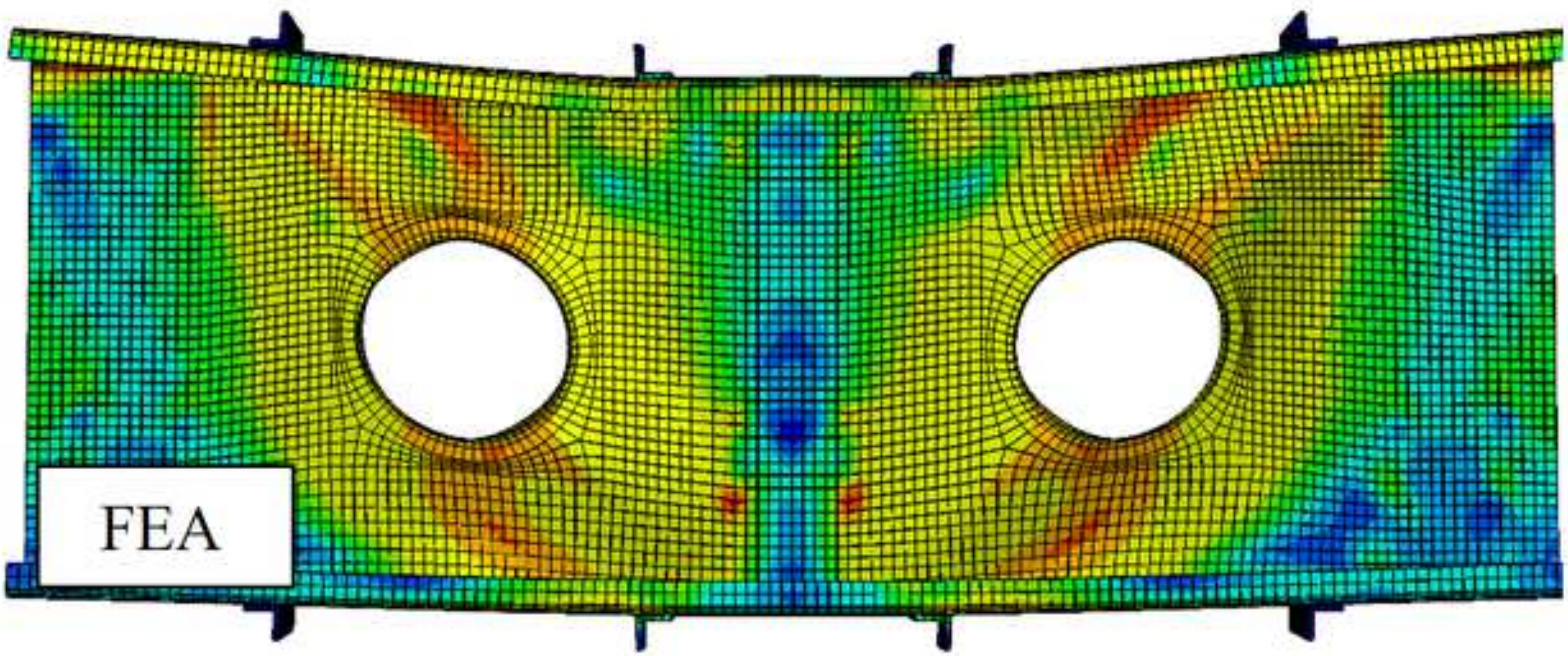

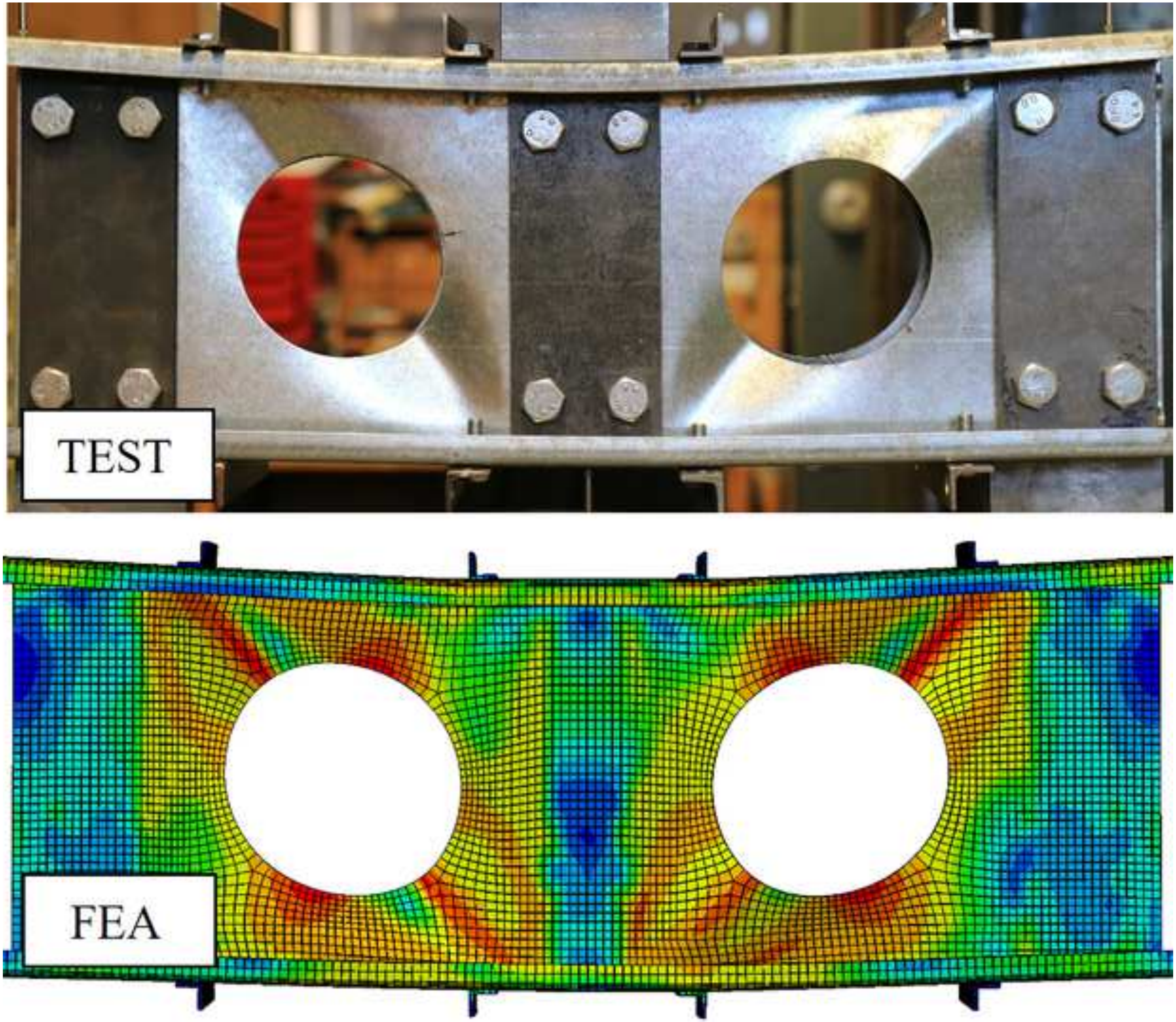
TEST
FEA

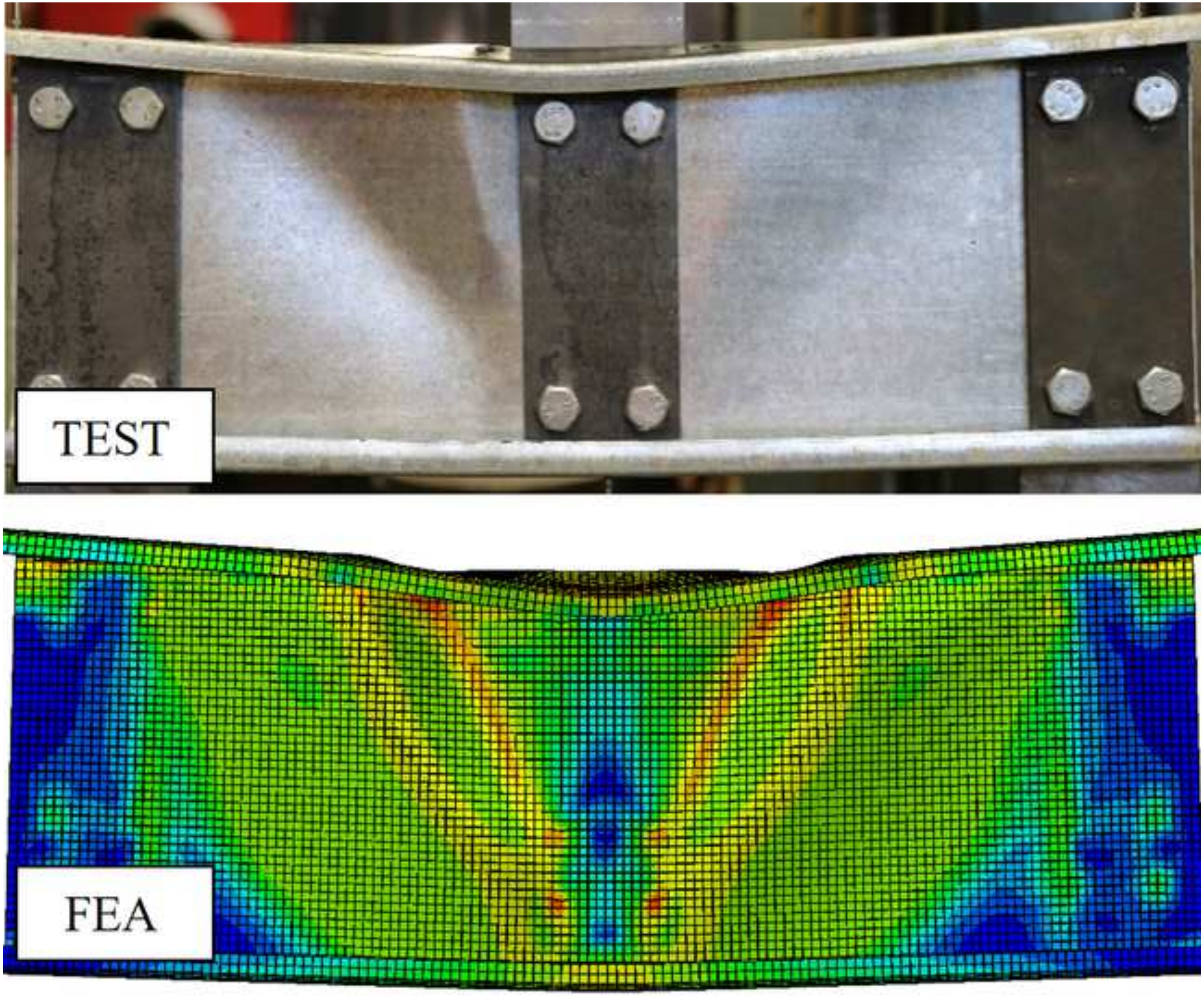
TEST
FEA

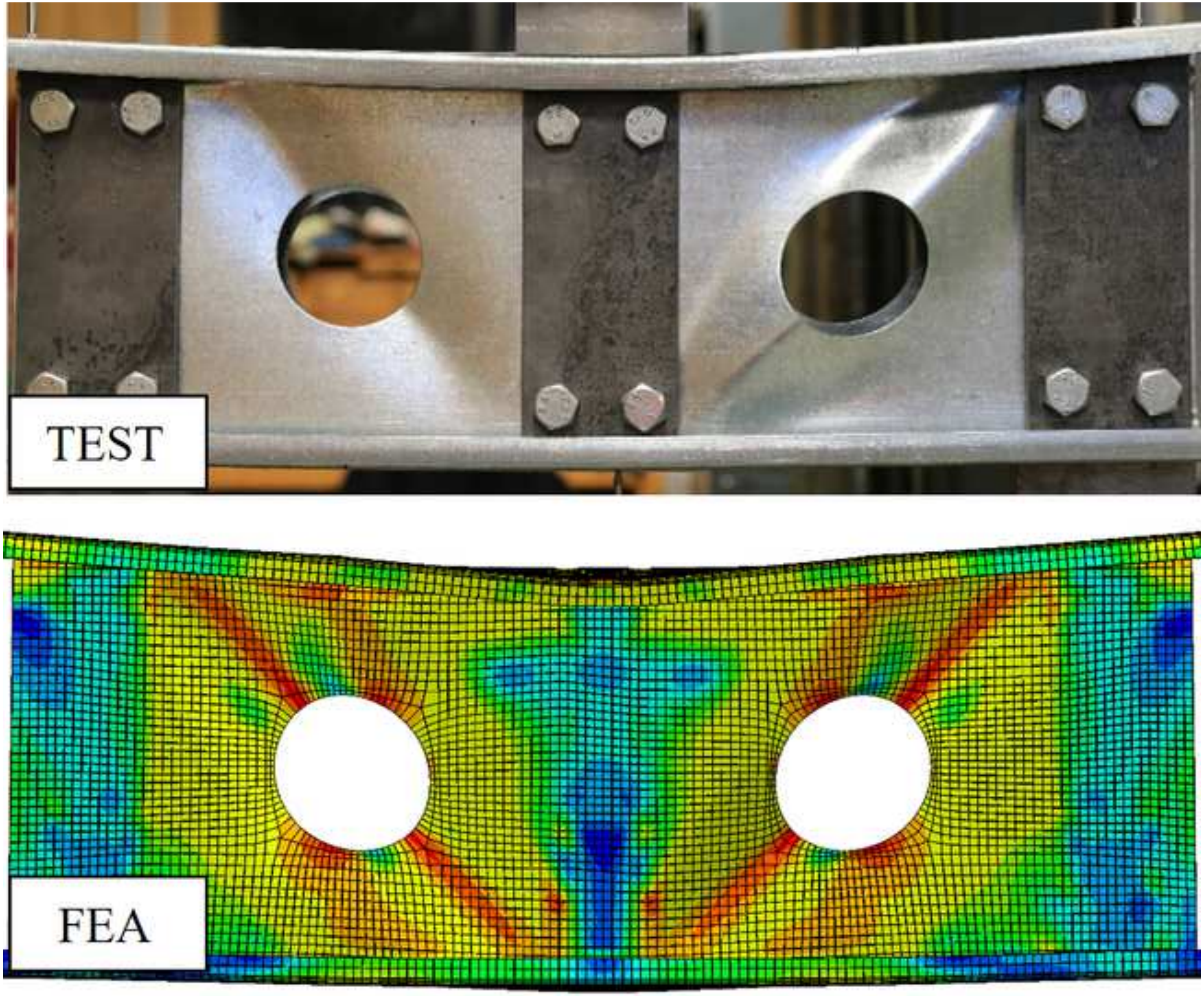
TEST
FEA

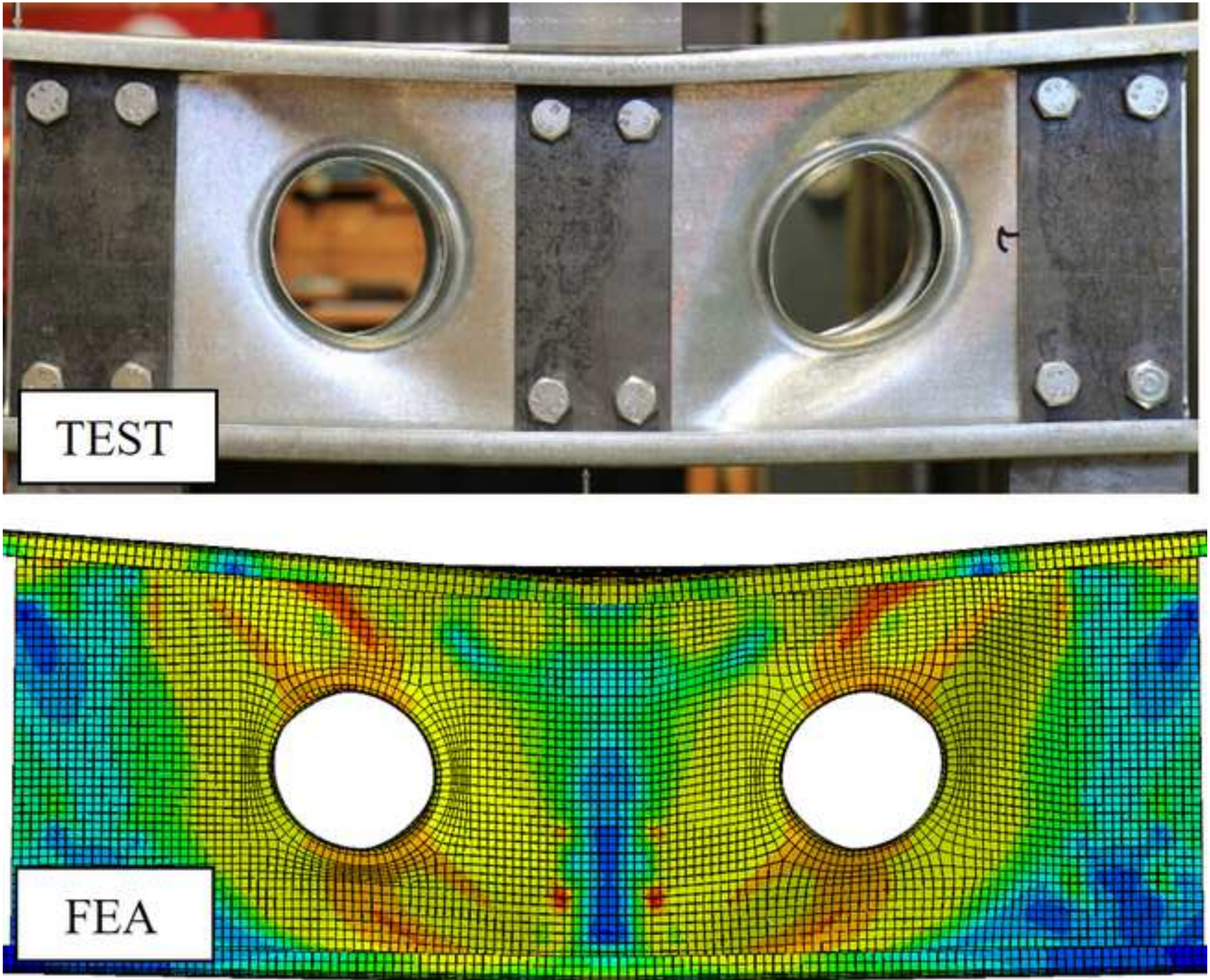
TEST
FEA

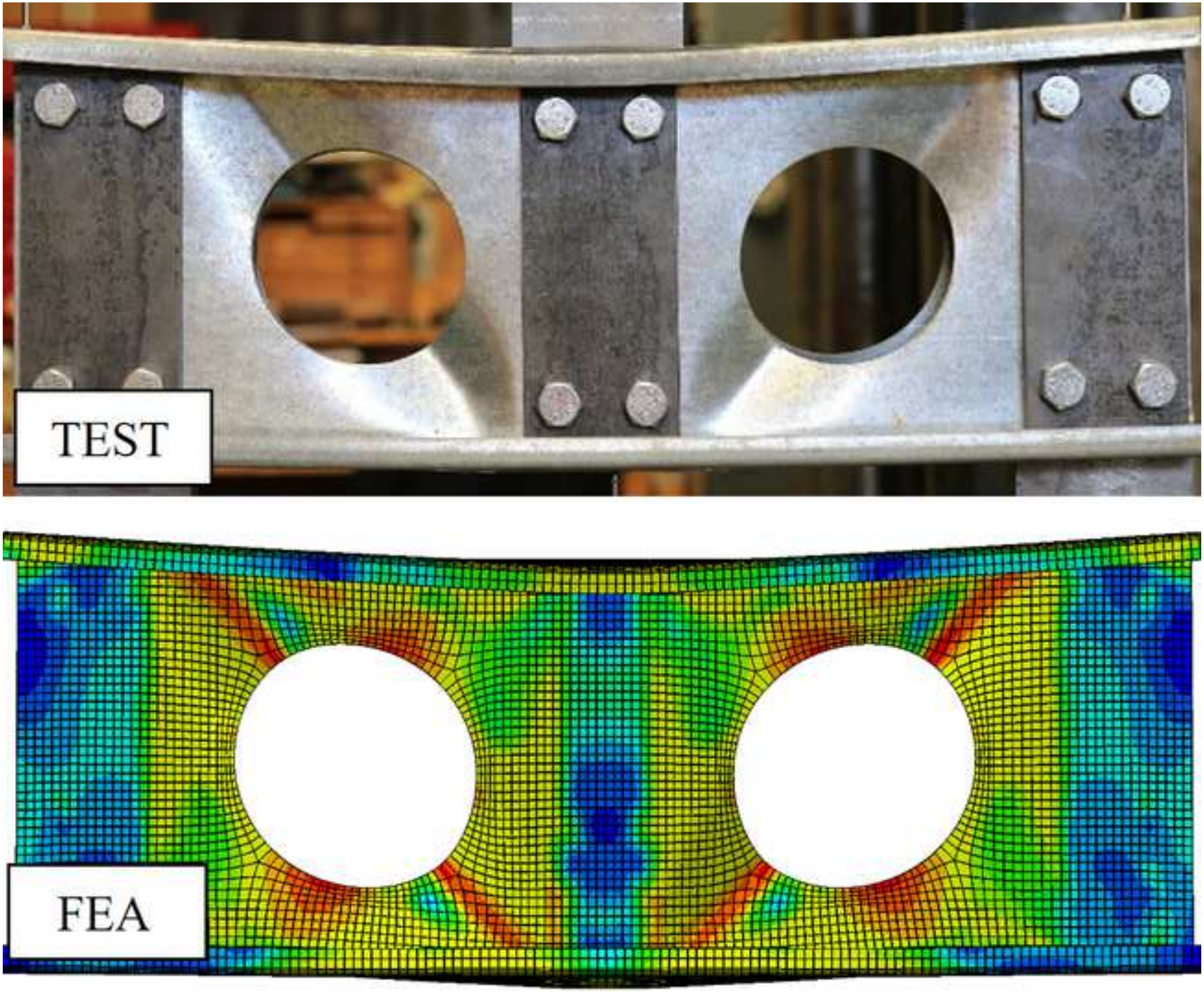
TEST
FEA

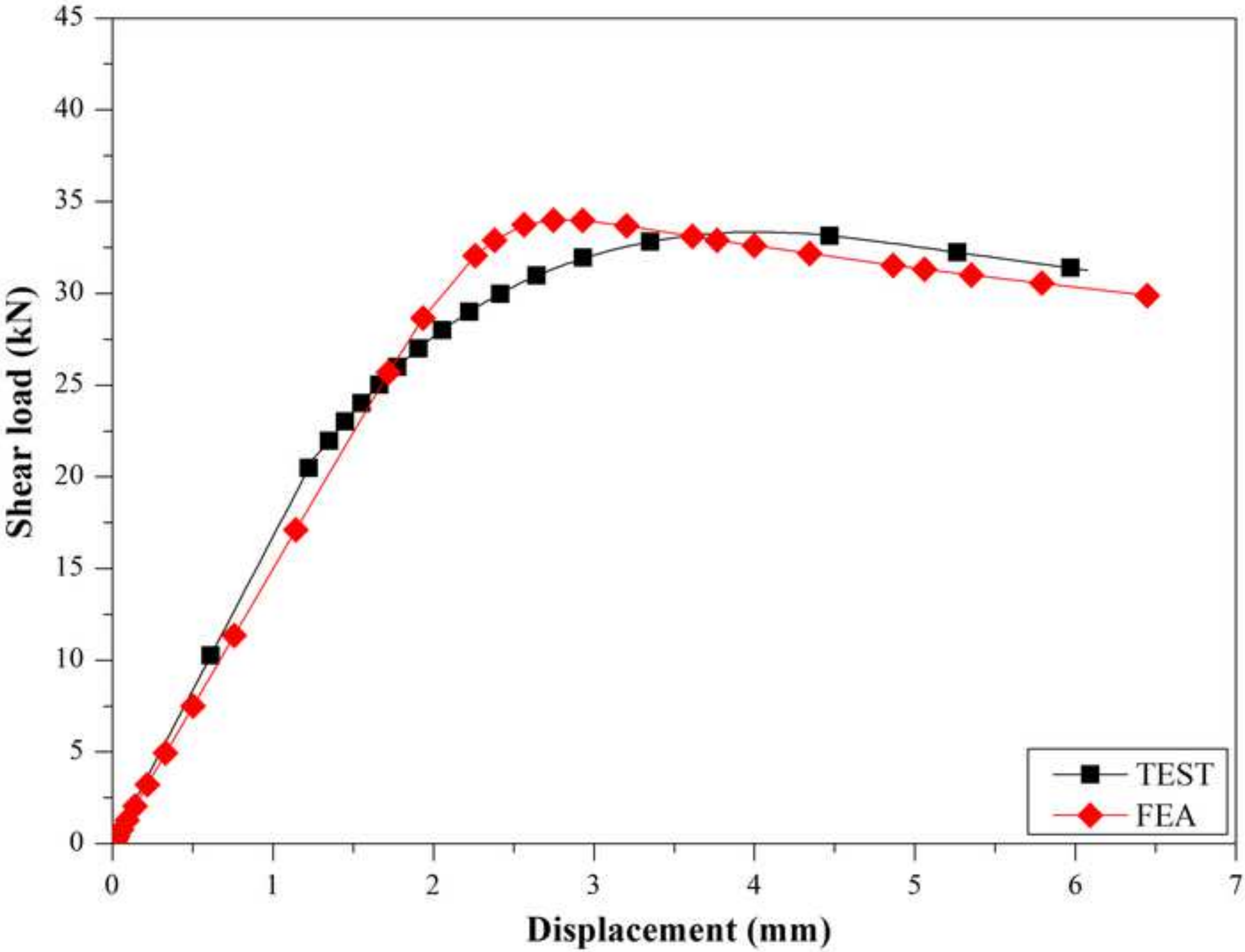
45
40
35
30
25
20
15
10
5
0
Shear load (kN)
0
1
2
3
4
5
6
7
Displacement (mm)
TEST
FEA

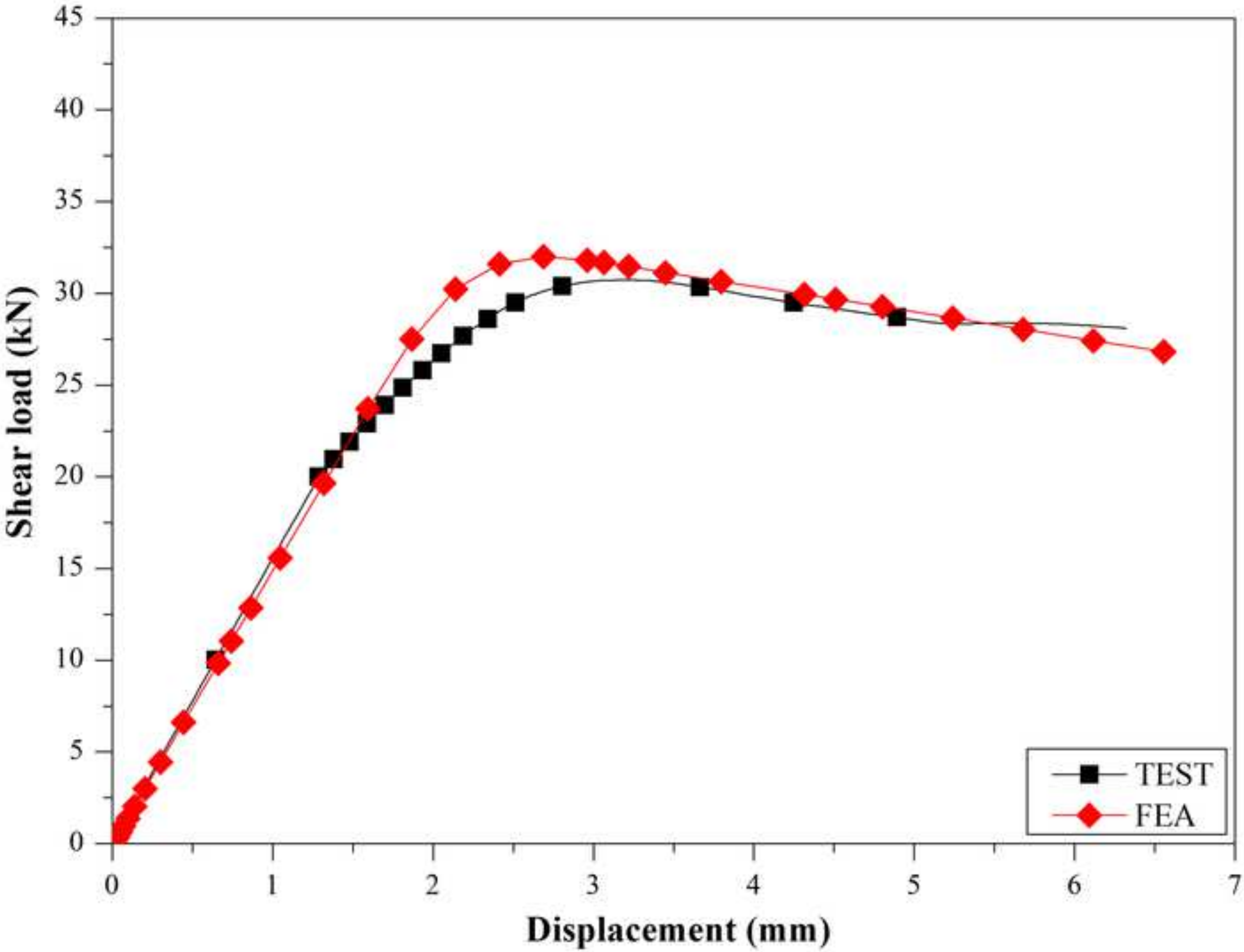
45
40
35
30
25
20
15
10
5
0
Shear load (kN)
0
1
2
3
4
5
6
7
Displacement (mm)
TEST
FEA

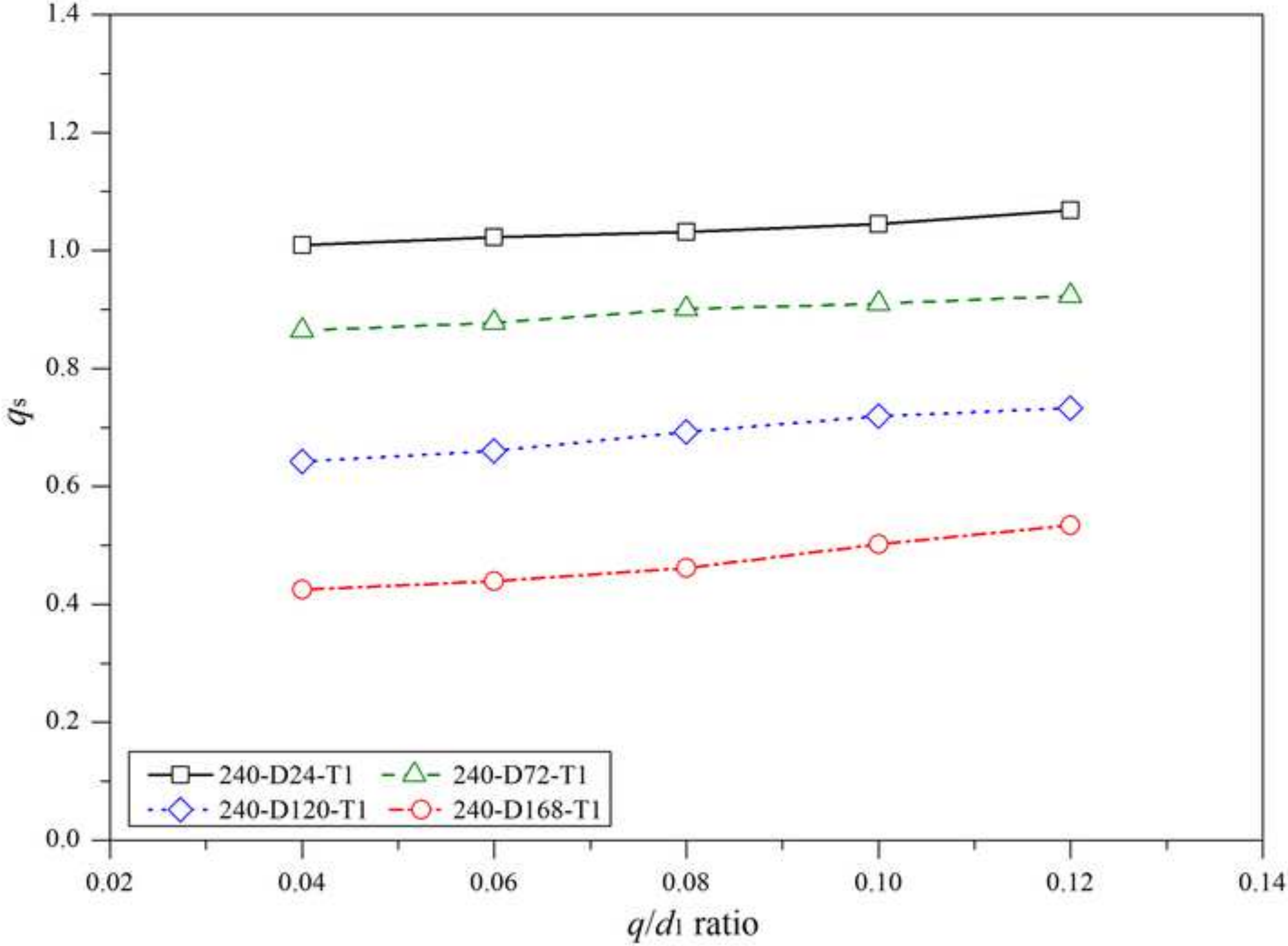

1.4
1.2
1.0
0.8
0.6
0.4
0.2
0.0
qs
0.02
0.04
0.06
0.08
0.10
0.12
0.14
q/d1 ratio
240-D24-T1
240-D72-T1
240-D120-T1
240-D168-T1

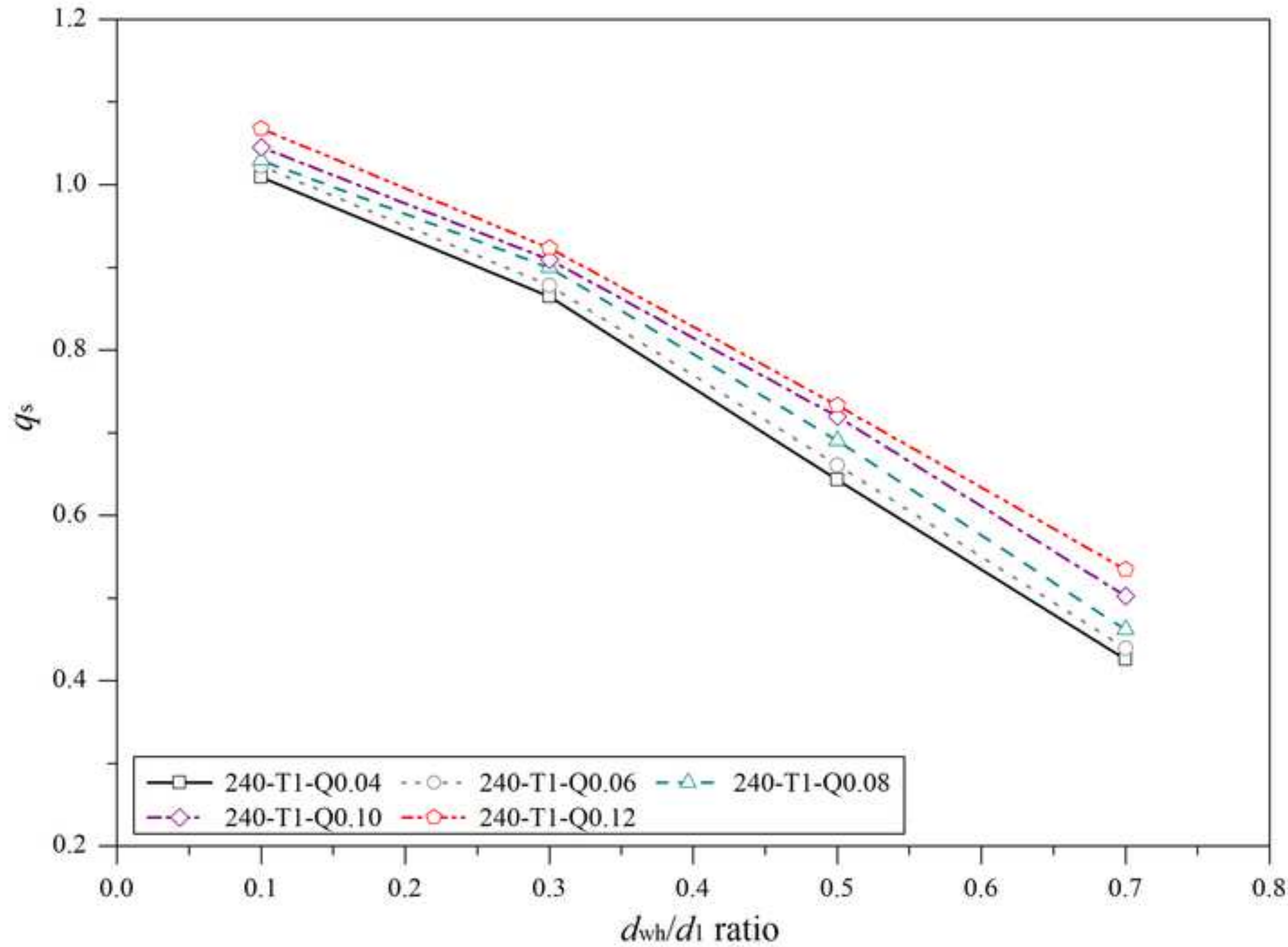

1.2
1.0
0.8
0.6
0.4
0.2
q_s
0.0
0.1
0.2
0.3
0.4
0.5
0.6
0.7
0.8
d_{wh}/d_1 ratio
240-T1-Q0.04
240-T1-Q0.06
240-T1-Q0.08
240-T1-Q0.10
240-T1-Q0.12

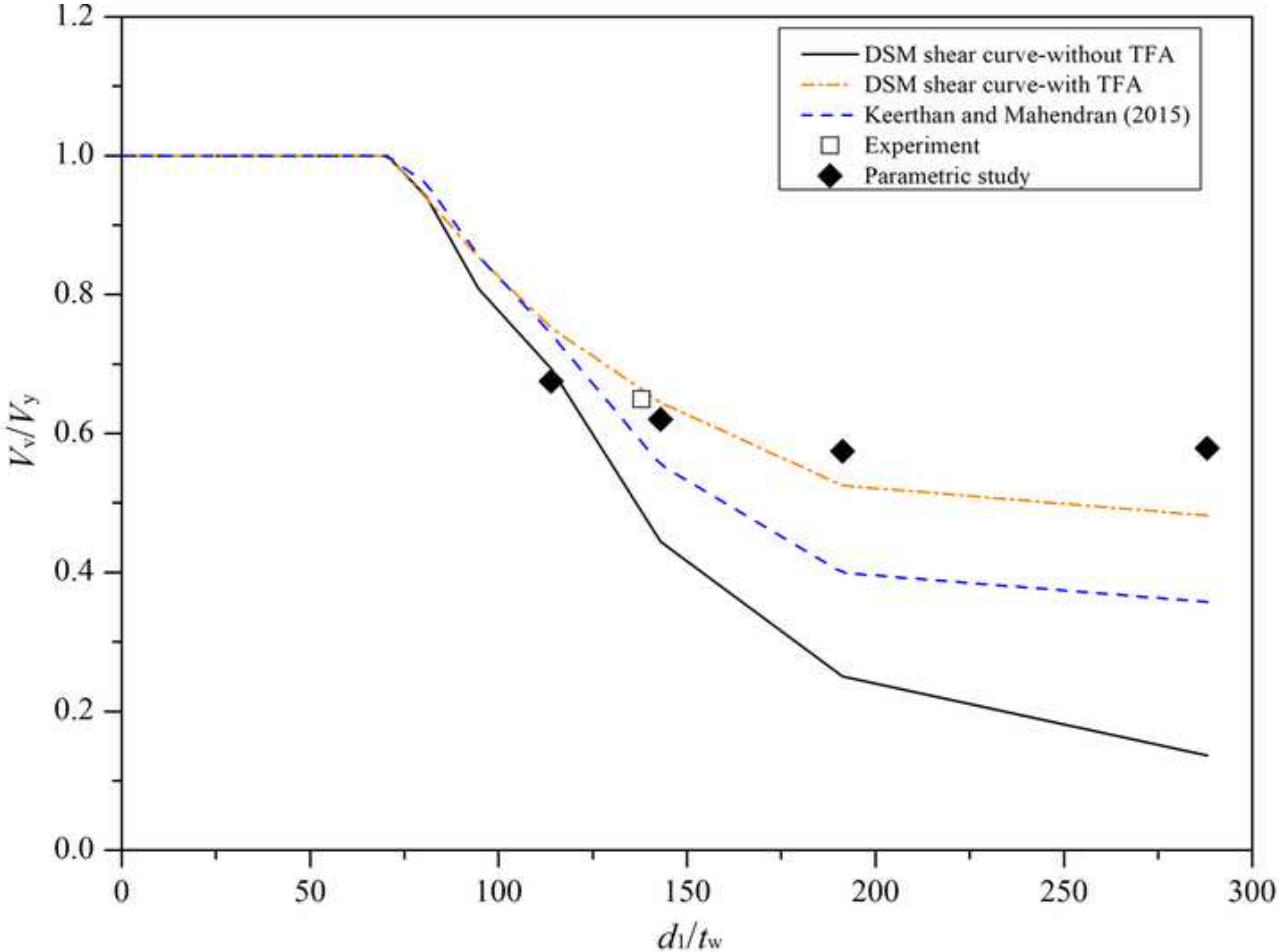

DSM shear curve-without TFA
DSM shear curve-with TFA
Keerthan and Mahendran (2015)
Experiment
Parametric study
V_v/V_y
d_1/t_w
0.0
0.2
0.4
0.6
0.8
1.0
1.2
0
50
100
150
200
250
300

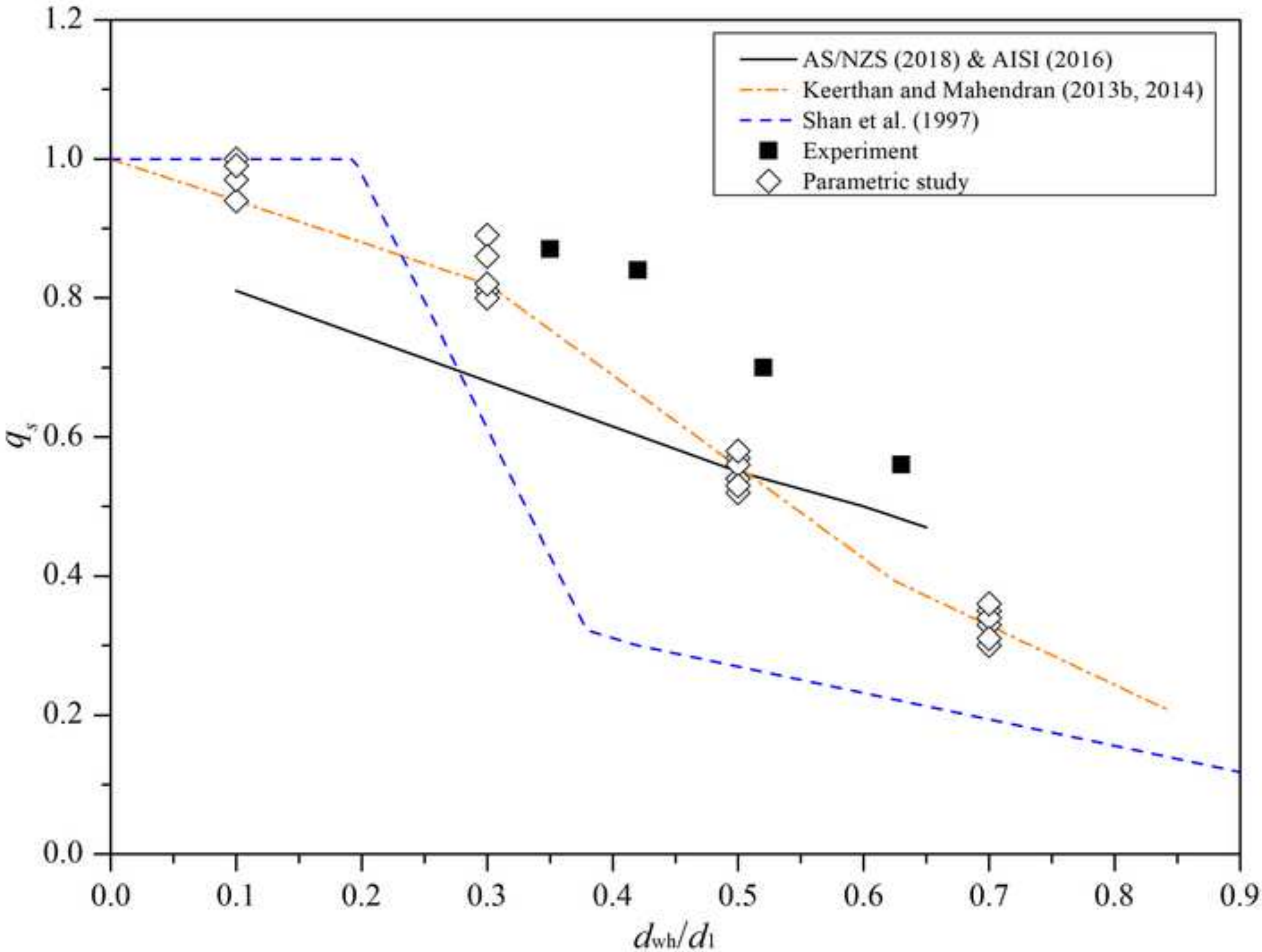

AS/NZS (2018) & AISI (2016)
Keerthan and Mahendran (2013b, 2014)
Shan et al. (1997)
Experiment
Parametric study
q_s
d_{wh}/d_1
0.0
0.2
0.4
0.6
0.8
1.0
1.2
0.0
0.1
0.2
0.3
0.4
0.5
0.6
0.7
0.8
0.9

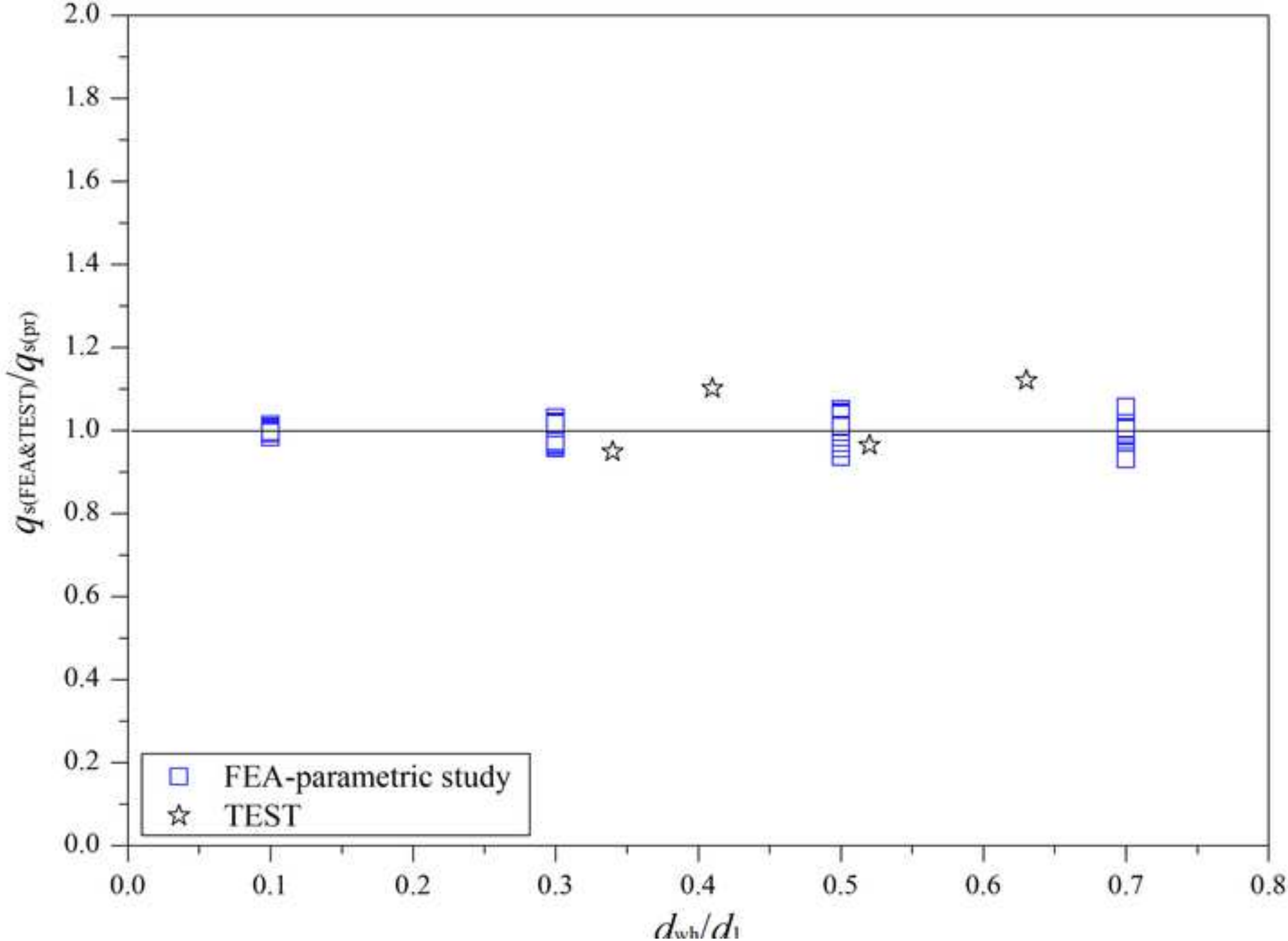
2.0
1.8
1.6
1.4
1.2
1.0
0.8
0.6
0.4
0.2
0.0
$q_{s(FEA\&TEST)}/q_{s(pr)}$
0.0
0.1
0.2
0.3
0.4
0.5
0.6
0.7
0.8
d_{wh}/d_1
FEA-parametric study
TEST

List of figures

(b) 240-A1.0-D90-UH-FR

(c) 240-A1.0-D140-EH-FR

(d) 240-A1.0-D140-UH-FR

(e) 240-A1.0-D0-NH-FU

(f) 240-A1.0-D90-UH-FU

(g) 240-A1.0-D140-EH-FU

(h) 240-A1.0-D140-UH-FU

Fig. 15. Comparison of FEA and experimental shear capacity versus displacement curves

(a) 240-A1.5-D90-UH-FR

(b) 240-A1.5-D90-UH-FU

Fig. 16. Effect of d_{wh}/d_1 and q/d_1 ratio on shear capacity reduction factor of channels with edge-stiffened web holes

(a) The effects of q/d1 ratio

(b) The effects of dwh/d1 ratio

Fig. 17. Comparison of test and FEA results with current shear design strengths for plain channels

Fig. 18. Comparison of test and FEA results with current shear design rules for channels with un-stiffened web holes (aspect ratio=1.0)

Fig. 19. Comparison of test and FEA results with proposed reduction factor equations for channels with edge-stiffened web holes